



HAL
open science

Testing the Recycled Gabbro Hypothesis for the Origin of "Ghost Plagioclase" Melt Signatures Using $^{87}\text{Sr}/^{86}\text{Sr}$ of Individual Olivine-Hosted Melt Inclusions from Hawai'i

Olivia E Anderson, M. G Jackson, Estelle F. Rose-Koga, J. P Marske, M. E Peterson, A. A Price, B. L Byerly, A.A. A Reinhard

► To cite this version:

Olivia E Anderson, M. G Jackson, Estelle F. Rose-Koga, J. P Marske, M. E Peterson, et al.. Testing the Recycled Gabbro Hypothesis for the Origin of "Ghost Plagioclase" Melt Signatures Using $^{87}\text{Sr}/^{86}\text{Sr}$ of Individual Olivine-Hosted Melt Inclusions from Hawai'i. *Geochemistry, Geophysics, Geosystems*, 2021, 22, 10.1029/2020GC009260 . hal-03164588

HAL Id: hal-03164588

<https://uca.hal.science/hal-03164588>

Submitted on 10 Mar 2021

HAL is a multi-disciplinary open access archive for the deposit and dissemination of scientific research documents, whether they are published or not. The documents may come from teaching and research institutions in France or abroad, or from public or private research centers.

L'archive ouverte pluridisciplinaire **HAL**, est destinée au dépôt et à la diffusion de documents scientifiques de niveau recherche, publiés ou non, émanant des établissements d'enseignement et de recherche français ou étrangers, des laboratoires publics ou privés.

1 **Testing the Recycled Gabbro Hypothesis for the Origin of "Ghost Plagioclase" Melt**
2 **Signatures Using $^{87}\text{Sr}/^{86}\text{Sr}$ of Individual Olivine-Hosted Melt Inclusions from Hawai'i**

3 **O. E. Anderson^{1*}, M. G. Jackson¹, E. F. Rose-Koga², J. P. Marske³, M. E. Peterson⁴, A. A.**
4 **Price¹, B. L. Byerly^{1,5}, A.A. Reinhard⁶**

5 ¹Isotope Geochemistry Facility – Center for Mantle Zoology, University of California Santa
6 Barbara, Department of Earth Science, Santa Barbara, CA, USA ²Université Clermont
7 Auvergne, CNRS, IRD Laboratoire Magmas et Volcans, OPGC, Clermont-Ferrand, France
8 ³Department of Terrestrial Magnetism, Carnegie Institution of Washington, Washington, DC,
9 USA ⁴AAAS Science and Technology Policy, ORISE Fellow hosted by the DOE, Washington,
10 DC, USA ⁵Thermo Fisher Scientific, Waltham, Massachusetts, USA, ⁶ Los Alamos National
11 Laboratory, Nuclear and Radiochemistry Group, Los Alamos, NM, USA

12 *Corresponding author: Olivia E. Anderson (anderson03@ucsb.edu)

13

14 **Key Points:**

- 15 • Hawaiian melt inclusions are variable in $^{87}\text{Sr}/^{86}\text{Sr}$, but are within the $^{87}\text{Sr}/^{86}\text{Sr}$ range of the
16 lavas from their host volcano.
- 17 • Mauna Loa melt inclusions with high $(\text{Sr}/\text{Ce})_{\text{N}}$ (ghost plagioclase) signatures have the
18 same $^{87}\text{Sr}/^{86}\text{Sr}$ as inclusions with normal $(\text{Sr}/\text{Ce})_{\text{N}}$.
- 19 • Diffusive interaction between rising melt and Hawaiian gabbros can produce the ghost
20 plagioclase signature in Mauna Loa melt inclusions.
21

22 Abstract

23 Melt inclusions with large, positive Sr anomalies have been described in multiple tectonic
24 settings, and the origins of this unusual geochemical feature are debated. Three origins have been
25 proposed involving plagioclase as the source of the elevated Sr: (i) direct assimilation of
26 plagioclase-rich lithologies, (ii) recycled lower oceanic gabbro in the mantle source, and (iii)
27 shallow-level diffusive interaction between present day lower oceanic crust (i.e., plagioclase-
28 bearing lithologies) and the percolating melt. A “ghost plagioclase” signature (i.e., a large,
29 positive Sr anomaly without associated high Al_2O_3) is present in melt inclusions from Mauna
30 Loa. We present new $^{87}\text{Sr}/^{86}\text{Sr}$ measurements of individual olivine-hosted melt inclusions from
31 three Hawaiian volcanoes, Mauna Loa, Loihi, and Koolau. The dataset includes a Mauna Loa
32 melt inclusion with the highest reported Sr anomaly (or highest $(\text{Sr}/\text{Ce})_N$, which is 7.2) for
33 Hawai'i. All melt inclusions have $^{87}\text{Sr}/^{86}\text{Sr}$ values within the range reported previously for the
34 lavas from each volcano. Critically, the $^{87}\text{Sr}/^{86}\text{Sr}$ of the high $(\text{Sr}/\text{Ce})_N$ melt inclusion lies within
35 the narrow range of Mauna Loa melts that lack high $(\text{Sr}/\text{Ce})_N$ signatures. To explain the high
36 $(\text{Sr}/\text{Ce})_N$ ratio of the ghost plagioclase signature using an ancient recycled gabbro would
37 therefore require the gabbro-infused mantle source to evolve, by chance, to have the same
38 $^{87}\text{Sr}/^{86}\text{Sr}$ as the source of the Mauna Loa melts that lack a recycled gabbro (ghost plagioclase)
39 signature. Alternatively, shallow-level diffusive interactions between Mauna Loa plagioclase-
40 rich cumulates and a percolating mantle-derived melt provides a simpler explanation for the
41 presence of the high $(\text{Sr}/\text{Ce})_N$ Mauna Loa melts.

42 1. Introduction

43 Melt inclusions, encapsulated within growing magmatic phenocrysts at depth, provide
44 “snapshots” of melt evolution that may not be preserved in whole rock compositions. One
45 geochemical signature found in melt inclusions is high Sr concentrations relative to trace
46 elements of similar incompatibility (such as Ce, Nd, and Sm). The magnitude of the Sr anomaly
47 can be quantified with the ratio $(\text{Sr}/\text{Ce})_N$ (where N signifies normalization to primitive mantle;
48 McDonough & Sun, 1995). Melt inclusions with high $(\text{Sr}/\text{Ce})_N$ ratios are significant because the
49 Sr anomaly found within these inclusions suggest plagioclase was involved in melt petrogenesis.
50 However, plagioclase accumulation, or assimilation, is not always obvious in the major element
51 chemistry of these melt inclusions (Danyushevsky et al., 2003, 2004; Gurenko & Chaussidon,
52 1995; Michael et al., 2002; Peterson et al., 2014; Saal et al., 2007; Slater et al., 2001; Sobolev et
53 al., 2000).

54 Melt inclusions with high $(\text{Sr}/\text{Ce})_N$ have been described from samples taken from mid-
55 ocean ridges (MORs; e.g., Danyushevsky et al., 2003, 2004; Michael et al., 2002) and hotspot
56 lavas erupted at ocean islands such as Galapagos (Peterson et al., 2014), Hawai'i (Sobolev et al.,
57 2000, 2011), and Iceland (e.g., Gurenko & Chaussidon, 1995; MacLennan, 2008; Slater et al.,
58 2001). A common geologic material with high $(\text{Sr}/\text{Ce})_N$ ratios is cumulate gabbro, which can be
59 a plagioclase-rich lithology. Its abundance in the deep oceanic crust represents the intrusive part
60 of the MOR sequence, and makes gabbro an obvious candidate for imparting large positive Sr
61 anomalies on percolating melts at MOR and ocean island settings (Peterson et al., 2014; Saal et
62 al., 2007; Sobolev et al., 2000; Yaxley & Sobolev, 2007). Plagioclase likely plays a central role
63 in generating large positive Sr anomalies because Sr is compatible in plagioclase compared to
64 elements of similar behavior (Sm, Nd) during peridotite melting and subsequent differentiation
65 in mafic magmatic systems.

66 Melts with large, positive Sr anomalies signal interaction with plagioclase-rich lithologies
67 like gabbro. Paradoxically, a subset of these high (Sr/Ce)_N melt inclusions lack coexisting
68 enrichments in major elements associated with plagioclase (e.g., Al), giving rise to the concept of
69 “ghost plagioclase” signatures in rare melt inclusions trapped in magmatic phenocrysts (Sobolev
70 et al., 2000). Three hypotheses invoked to explain the rare occurrences of large, positive Sr
71 anomalies in melt inclusions include: (i) direct assimilation of gabbro by upwelling melts
72 (Danyushevsky et al., 2003), (ii) melts of recycled lower oceanic (gabbroic) crust in the mantle
73 source that are hybridized with peridotite and trapped as melt inclusions in growing magmatic
74 phenocrysts (Chauvel & Hémond, 2000; Hofmann & Jochum, 1996; Sobolev et al., 2000;
75 Yaxley & Sobolev, 2007), and (iii) diffusive interaction between percolating melt and a
76 plagioclase-rich crystal mush (Peterson et al., 2014; Saal et al., 2007).

77 Direct assimilation has been ruled out to explain Sr anomalies in many oceanic hotspot
78 melt inclusions from Hawai'i (Sobolev et al., 2000) and Galapagos (Peterson et al., 2014)
79 because the ghost plagioclase melt inclusions have large, positive Sr anomalies that do not have
80 corresponding elevated Al₂O₃, as would be expected for direct assimilation of Al-rich
81 plagioclase (e.g., Peterson et al., 2014; Sobolev et al., 2000).

82 Regarding the second hypothesis, melts of recycled gabbroic lower oceanic crust may
83 generate trace element chemistry similar to many high (Sr/Ce)_N inclusions from ocean islands.
84 The recycled gabbro model suggests eclogite, metamorphosed gabbroic material, would partially
85 melt earlier (deeper) than surrounding peridotite in an upwelling mantle plume (Sobolev et al.,
86 2000; Yaxley & Sobolev, 2007). The melt of the eclogite is silicic (e.g., dacitic) and thus would
87 react with surrounding peridotite, producing garnet-bearing pyroxenites (Yaxley & Green, 1998).
88 The large, positive Sr anomaly is transferred from the silicic melt to the reacted pyroxenite and
89 resides mainly within clinopyroxene. When the reacted pyroxenite partially melts during
90 continued plume upwelling, high-MgO liquids with elevated Sr are generated and mix with
91 normal melts formed by partial melting of peridotite. In the recycled gabbro melting model, the
92 Sr budget in a high (Sr/Ce)_N melt will be dominated by Sr from the gabbro, because the
93 peridotite in the melt source of this model is not assumed to have a large, positive Sr anomaly.
94 As a result, this model predicts that Mauna Loa melt inclusions with large, positive Sr anomalies
95 will have essentially the same ⁸⁷Sr/⁸⁶Sr as the recycled gabbro.

96 The third hypothesis predicts that diffusive interaction between percolating melt and
97 plagioclase-rich mush will produce trace element patterns reflecting a gabbro contribution. Due
98 to the slow diffusive nature of major elements (e.g., Al₂O₃), the diffusion model will not generate
99 significant changes in the major element concentration of a melt. In addition, diffusive
100 interaction will cause the high (Sr/Ce)_N melt inclusions to have the same Pb (Peterson et al.,
101 2014) and Sr (this study) isotopic composition as the gabbro through which they percolated
102 (because Sr and Pb have high diffusivities in plagioclase). If the melt percolated through and
103 interacted with the gabbro of the ~100 Ma (Müller et al., 2008) MOR crust beneath Hawai'i, melt
104 inclusions will adopt ⁸⁷Sr/⁸⁶Sr of the relatively modern MOR crust. Conversely, if the melt
105 inclusions with high (Sr/Ce)_N result from interaction with gabbroic mush in a Mauna Loa magma
106 chamber, these inclusions will have ⁸⁷Sr/⁸⁶Sr that is indistinguishable from lavas erupted at
107 Mauna Loa. In both cases (i.e., MOR gabbro or Mauna Loa gabbro), the resulting ⁸⁷Sr/⁸⁶Sr ratio
108 of high (Sr/Ce)_N melt inclusions is predicted to be indistinguishable from the ⁸⁷Sr/⁸⁶Sr of the
109 gabbro with which the percolating melt interacted.

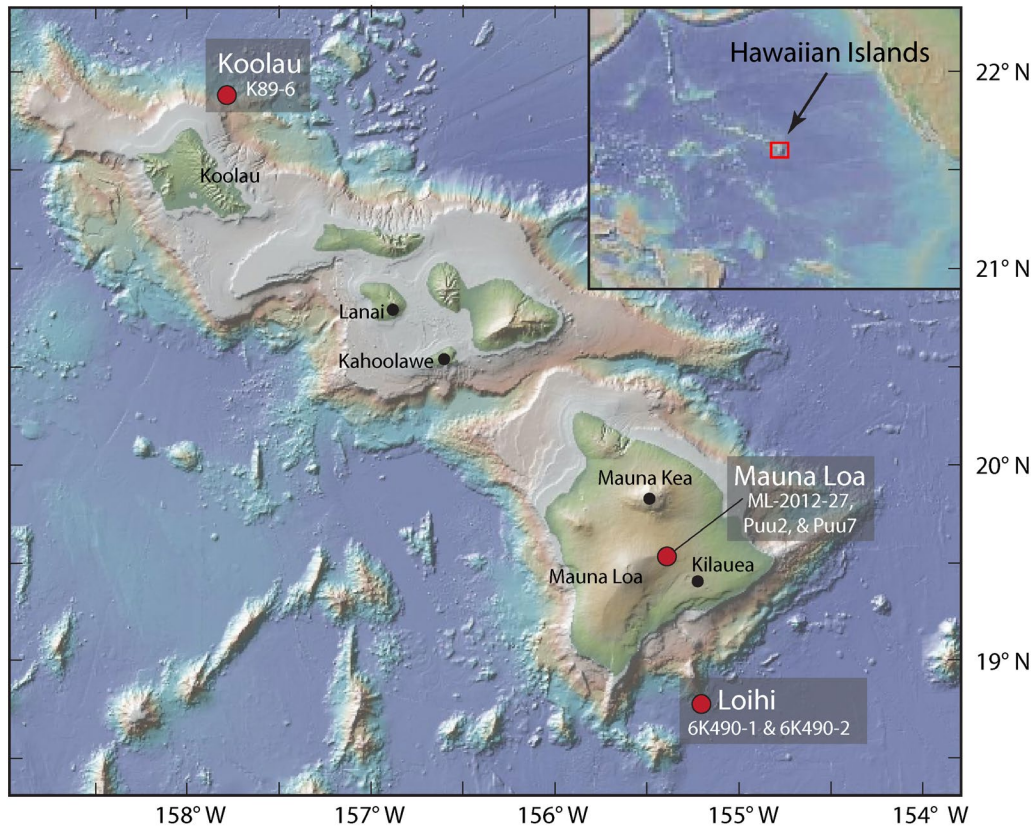


Figure 1. Map of the Hawaiian Islands showing sample locations (red dots) for the six samples in this study: two from Loihi, three from Mauna Loa, and one from Koolau. The three Mauna Loa samples (red dot on Mauna Loa), and the two Loihi samples (red dot on Loihi) are located very close geographically and are represented by a single symbol. Black dots mark the volcanoes that are used for comparison in this study. Map was created using GeoMapApp (geomapapp.org).

110 This study presents strontium isotopes measured on melt inclusions with high $(\text{Sr}/\text{Ce})_{\text{N}}$ to
 111 distinguish between the two hypotheses—diffusive interaction between percolating melt and
 112 modern plagioclase-rich mush versus melts of ancient recycled gabbro—for generating “ghost
 113 plagioclase” signatures in melt inclusions. In addition, major, volatile (Cl and S), and trace
 114 element concentrations are included for individual melt inclusions isolated from six different
 115 lavas from three Hawaiian volcanoes: Mauna Loa, Loihi, and Koolau. One of the melt inclusions
 116 from Mauna Loa reported here has the highest $(\text{Sr}/\text{Ce})_{\text{N}}$ (7.2) ratio ever reported in a Hawaiian
 117 lava or melt inclusion.

118 2. Methods

119 Olivine-hosted melt inclusions and glasses from six Hawaiian picrites from Mauna Loa
 120 (samples Puu2, Puu7, and ML-2012-27), Loihi (samples 6K490-1 and 6K490-2), and Koolau
 121 (sample K89-6; Figure 1) were analyzed. Melt inclusions in this study were not homogenized, as
 122 most melt inclusions analyzed were naturally glassy, and characterized for $^{87}\text{Sr}/^{86}\text{Sr}$ and
 123 elemental concentrations. However, five inclusions (Puu2-1-2, Puu7-2-15, Puu7-2-92b, K89-
 124 6_52, 6K490-1_51) were partially crystalline and were characterized only for $^{87}\text{Sr}/^{86}\text{Sr}$, and not
 125 for elemental concentrations.

126 The Supplement describes the samples selected, melt inclusion preparation methods,
 127 including grinding the olivines into tiny (several hundred microns on a side) cubes to remove all

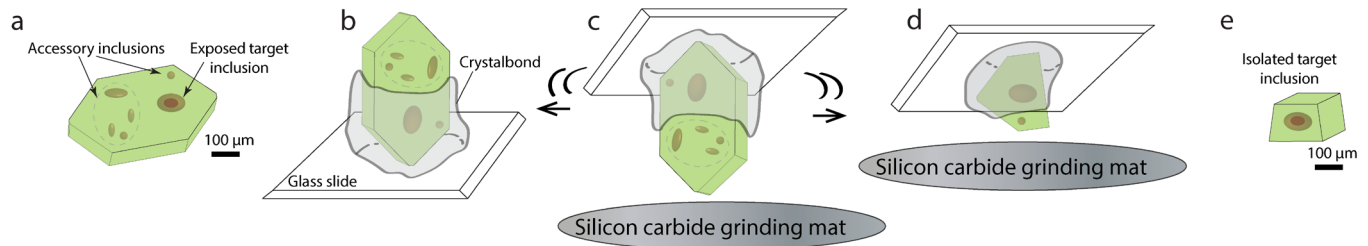


Figure 2. Method for isolating individual olivine-hosted melt inclusions. **(a)** Olivines often have multiple melt inclusions and all except for the target melt inclusion must be removed prior to sample leaching and dissolution. First, the target inclusion is exposed, the host olivine is mounted in epoxy, and the melt inclusion is analyzed for major, trace, and volatile elements using *in situ* techniques. **(b)** After *in situ* analysis, accessory melt inclusions are removed by mounting the olivine grain onto a glass slide using Crystalbond™. **(c)** The olivine is then ground on silicon carbide grinding mats until the accessory melt inclusions on one side of the olivine grain are removed. **(d)** The olivine grain is reoriented to optimally remove remaining accessory melt inclusions, and this process is repeated until only the target melt inclusion is left within a case of its olivine host **(e)**. The “cubed” melt inclusion is then leached and cleaned in ultra-pure acid before dissolution and column chemistry.

128 accessory inclusions within an olivine grain (Figure 2), thereby isolating the melt inclusion of
 129 interest. The Supplement also includes detailed major (electron microprobe), volatile (electron
 130 microprobe and ion probe), and trace (laser ablation ICP-MS) element analytical techniques of
 131 melt inclusions, host olivines, and host pillow glass/tephra. Finally, the Supplement includes
 132 details of Sr separation chemistry for melt inclusions, and $^{87}\text{Sr}/^{86}\text{Sr}$ analyses by thermal
 133 ionization mass spectrometry (TIMS) at the University of California, Santa Barbara Isotope
 134 Geochemistry Facility.

135 3. Results

136 The melt inclusions are hosted in olivine crystals ranging from $\text{Fo}_{80.4}$ to $\text{Fo}_{90.1}$ (Table S1).
 137 Melt inclusions span a wide range of sizes, most having maximum major axis lengths between
 138 120 and 630 μm (Figure S3). A high, positive Sr anomaly can be quantified using $(\text{Sr}/\text{Ce})_{\text{N}}$.
 139 Below we group the melt inclusions from Mauna Loa (including this study) into two sets: High
 140 $(\text{Sr}/\text{Ce})_{\text{N}}$ inclusions (with $(\text{Sr}/\text{Ce})_{\text{N}} > 2$), and normal-type melt inclusions (with $(\text{Sr}/\text{Ce})_{\text{N}}$ between
 141 0.8 and 1.3, and excluding the ultra-calcic melt inclusion). Three Pu'u Wahi melt inclusions
 142 (samples Puu7-2-15, Puu7-2-92b, and Puu2-1-2), and one melt inclusion each from Koolau
 143 (sample K89-6_52) and Loihi (sample 6K490-1_51), are partially crystalline. Partially crystalline
 144 inclusions are not included in major and trace element plots as crystallization can modify major
 145 and trace element concentrations, but they are included within the $^{87}\text{Sr}/^{86}\text{Sr}$ dataset.

146 In a plot of Al_2O_3 versus MgO (Figure 3), the highest $(\text{Sr}/\text{Ce})_{\text{N}}$ melt inclusion from
 147 Mauna Loa is shown with new data on normal-type melt inclusions and previously published
 148 Mauna Loa melt inclusions (Reinhard et al., 2018; Sobolev et al., 2000, 2011) and Hawaiian
 149 whole rock and glass data (Frey et al., 2016; Garcia et al., 1993, 1995, 1998). Frey et al. (2016)
 150 compiled a dataset of Hawaiian shield-stage lavas and provides a high-quality dataset of major
 151 and trace elements and $^{87}\text{Sr}/^{86}\text{Sr}$ compositions for comparison to the lavas and melt inclusions in
 152 this study. The melt inclusions presented here, including the highest $(\text{Sr}/\text{Ce})_{\text{N}}$ melt inclusion,
 153 have Al_2O_3 concentrations similar to the host glasses and plot on, or close to, the array formed by
 154 Hawaiian lavas (the exception is a single ultra-calcic melt inclusion which has ~2 wt.% lower
 155 concentration of Al_2O_3 than the Hawaiian array at the same MgO content). Gabbroic xenoliths

156 from Mauna Loa (sampling the deep recesses of Mauna Loa volcano; Gaffney, 2002), and
157 gabbros from the Gabal Gerf ophiolite (Zimmer et al., 1995), plot above the array formed by
158 Hawaiian melt inclusions and whole rocks. Critically, the highest $(\text{Sr}/\text{Ce})_{\text{N}}$ melt inclusion (ML-
159 2012-27_19b) is not shifted off of the Hawaiian array toward the gabbroic compositions.

160 Melt inclusions have major element characteristics consistent with Hawaiian whole rock
161 and glass data reported in the literature (Figure S4). In general, melt inclusions have lower FeO_t
162 (total iron as FeO) compared to their host glass, which is similar to olivine-hosted melt
163 inclusions from other localities that have experienced post-entrapment Fe-Mg diffusive exchange
164 (Danyushevsky et al., 2000; Gaetani & Watson, 2000; Kent, 2008; Sobolev & Danyushevsky,
165 1994). Some of the Mauna Loa inclusions have high CaO relative to the Hawaiian lava array,
166 including a single ultra-calcic melt inclusion reported here (sample Puu2-1-39, seen most clearly
167 in the panel showing $\text{CaO}/\text{Al}_2\text{O}_3$ versus MgO in Figure S4f), consistent with previous findings of
168 high CaO melts at Hawai'i (Huang & Humayun, 2016; Kogiso & Hirschmann, 2001). While
169 some melt inclusions in this study have slightly different major element compositions that trend
170 outside of the field defined by Hawaiian lavas (Figure S4), below we show that none of the melt
171 inclusions have unusual $^{87}\text{Sr}/^{86}\text{Sr}$ that varies outside of the range found in whole rocks and
172 glasses at each respective volcano.

173 The Mauna Loa melt inclusions from Pu'u Wahi reported here have a range of $(\text{Sr}/\text{Ce})_{\text{N}}$
174 of 0.8–1.5, and the ML-2012-27 Mauna Loa melt inclusions reported here have a $(\text{Sr}/\text{Ce})_{\text{N}}$ range
175 of 1.0–7.2 (Figures 3 and 4), where $(\text{Sr}/\text{Ce})_{\text{N}}$ of 7.2 is the highest value reported for any Mauna
176 Loa melt inclusion. Sobolev et al. (2000, 2011) reported $(\text{Sr}/\text{Ce})_{\text{N}}$ values up to 5.4, with 11
177 inclusions that have $(\text{Sr}/\text{Ce})_{\text{N}} > 2$. In a plot of $(\text{Sr}/\text{Ce})_{\text{N}}$ versus Al_2O_3 (Figure 3), the highest

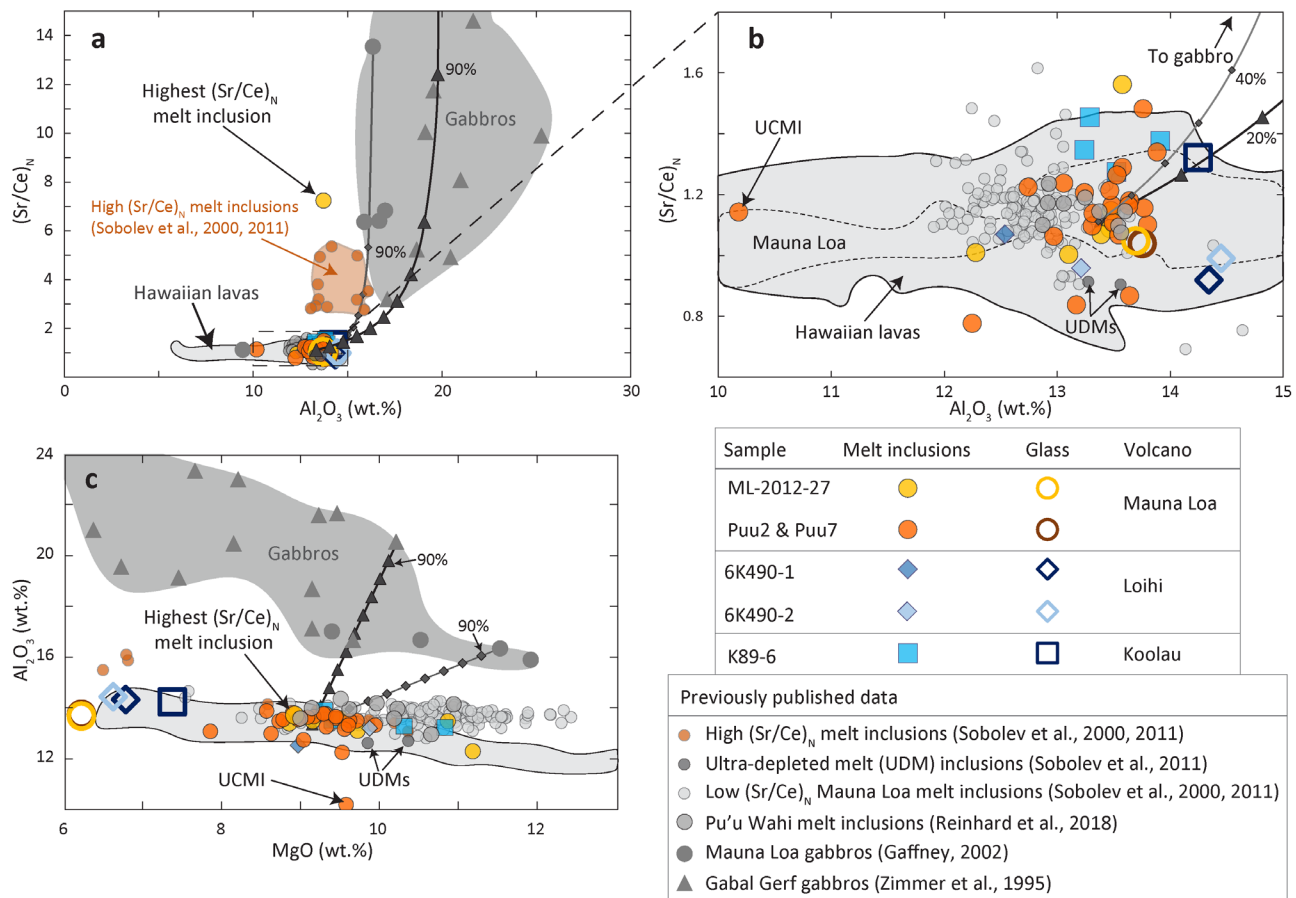


Figure 3. High (Sr/Ce)_N Hawaiian melt inclusions and host pillow/tephra glasses compared to Hawaiian lavas, and to Mauna Loa and Gabal Gerf gabbros. **(a)** In (Sr/Ce)_N versus Al₂O₃ (wt.%) space, the melt inclusion data do not show a positive correlation. A mixing model (line with filled diamonds) is shown between the average Pu'u Wahi melt inclusion composition from this study (Table S10) and the Mauna Loa gabbro with the highest (Sr/Ce)_N (sample 98-65, with (Sr/Ce)_N = 13.5) from Gaffney (2002), with 10% increments marked; a second mixing model (line with filled triangles) is shown between the average Pu'u Wahi melt inclusion composition (Table S10) and the Gabal Gerf gabbro with the highest (Sr/Ce)_N (sample GG36, with (Sr/Ce)_N = 148) from Zimmer et al. (1995). **(b)** The same plot as in (a) except expanded to highlight melt inclusions with (Sr/Ce)_N < 2. **(c)** In Al₂O₃ (wt.%) versus MgO (wt.%) space; the mixing model uses the same mixing endmembers as panels (a) and (b). We use the comprehensive Hawaiian dataset (which includes both whole rock and glass analyses) from Frey et al. (2016) for comparison because it provides a compilation of the highest-quality major and trace element data from Hawai'i. The Frey et al. (2016) dataset has been filtered as described in Section S1.5 of the Supplementary Methods. Loa-trend volcanoes (Loihi, Mauna Loa, Koolau, Lanai, and Kahoolawe) and Kea-trend volcanoes (Mauna Kea and Kilauea) from the Frey et al. dataset are shown here. The tephra/pillow glass for each sample hosting melt inclusions is also shown for reference. The Pu'u Wahi tephra glass major and trace element concentrations are from Sobolev et al. (2011). Low (Sr/Ce)_N Mauna Loa melt inclusions from Sobolev et al. (2000, 2011) include inclusions with (Sr/Ce)_N < 2. Concentrations shown in the figure have been corrected for addition or subtraction of equilibrium olivine so that the melt inclusions are in equilibrium with the host olivine. Only data for glassy melt inclusions are shown. The two ultra-depleted melt (UDM) inclusions from Sobolev et al. (2011) are identified. An outlier with low Al₂O₃ content, which is an ultra-calcic melt inclusion (UCMI) from Pu'u Wahi, is noticeable in all three panels.

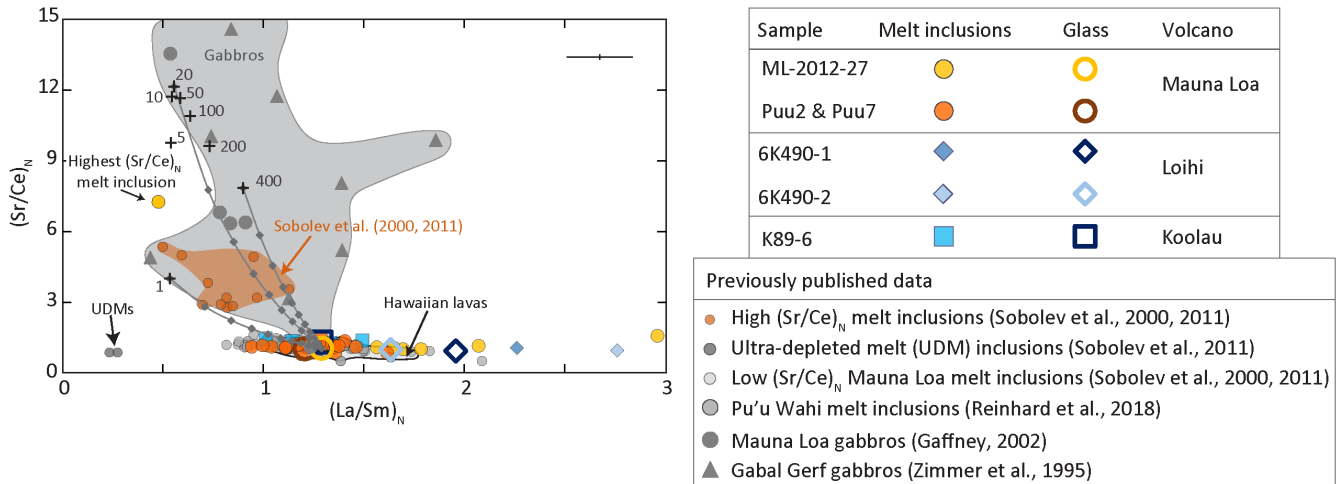


Figure 4. $(\text{Sr}/\text{Ce})_N$ versus $(\text{La}/\text{Sm})_N$ plot shows the diffusive interaction model results (black crosses) for Mauna Loa based on the Peterson et al. (2014) model, and the numbers next to the data points represent the number of years of diffusion. Mixing lines are shown between the ML-2012-27 host tephra composition (Table S8) and compositions generated at 1, 20, and 400 years of diffusive interaction. Average 2σ error bars are shown in the top right corner of plot.

179 melt inclusions with lower $(\text{Sr}/\text{Ce})_N$.

180 In a plot of $(\text{Sr}/\text{Ce})_N$ versus $(\text{La}/\text{Sm})_N$ (Figure 4), the high $(\text{Sr}/\text{Ce})_N$ inclusions, all of
 181 which are from Mauna Loa, tend to have lower $(\text{La}/\text{Sm})_N$ ratios than normal-type melt inclusions
 182 and Hawaiian lavas, which is consistent with prior observations at Hawai'i (Sobolev et al., 2000)
 183 and Galapagos (Peterson et al., 2014). Excluding the ultra-depleted melt (UDM) inclusions from
 184 Sobolev et al. (2011), the melt inclusion with the highest $(\text{Sr}/\text{Ce})_N$ has the lowest $(\text{La}/\text{Sm})_N$
 185 observed in Hawaiian melts. Like other high $(\text{Sr}/\text{Ce})_N$ inclusions from Hawai'i, the high $(\text{Sr}/\text{Ce})_N$
 186 inclusion is depleted in light rare earth elements (REEs) relative to middle REEs, an observation
 187 that has been made before at Hawai'i (e.g., Sobolev et al., 2000) and Galapagos (Peterson et al.,
 188 2014). Notably, all Hawaiian melt inclusions with high $(\text{Sr}/\text{Ce})_N$ in this study are hosted in
 189 Mauna Loa lavas; none of the Loihi or Koolau samples have large positive $(\text{Sr}/\text{Ce})_N$, but we note
 190 that fewer Loihi and Koolau melt inclusions have been characterized.

191 Mauna Loa melt inclusions reported here have some variability in trace element ratios.
 192 Primitive mantle (McDonough & Sun, 1995) normalized trace element patterns (spidergrams) of
 193 all glassy melt inclusions reported in this study are shown together with spidergrams of the host
 194 glass or tephra (Figure 5a–d). The highest $(\text{Sr}/\text{Ce})_N$ inclusion exhibits the most significant
 195 deviation in pattern shape (with overall depletion in incompatible trace element abundances
 196 compared to the other Mauna Loa inclusions). For comparison, the Mauna Loa gabbro with the
 197 highest $(\text{Sr}/\text{Ce})_N$ (sample 98-65; Gaffney, 2002) is plotted against Mauna Loa sample ML-2012-
 198 27 (Figure 5). The highest $(\text{Sr}/\text{Ce})_N$ inclusion has a similar spidergram to high $(\text{Sr}/\text{Ce})_N$
 199 inclusions from Sobolev et al. (2000, 2011), but different compared to the average normal Pu'u
 200 Wahi melt inclusion (Figure S5). Pu'u Wahi melt inclusions from Mauna Loa reported in
 201 Reinhard et al. (2018) are plotted alongside this study's Pu'u Wahi inclusions, and they exhibit
 202 less variability in spidergram patterns than the Mauna Loa ML-2012-27 inclusions. Similarly, the

203 spidergrams for the Loihi and Koolau inclusions show relatively little variability and are similar
204 to the host glass.

205 Figure 5 also shows that the Mauna Loa gabbros from Gaffney (2002) contain positive Pb
206 anomalies whereas the Mauna Loa melt inclusions have negative Pb anomalies. Sulfides are
207 observed in Hawaiian lavas (Stone & Fleet, 1991). If sulfides are responsible for the positive Pb
208 anomalies in Mauna Loa gabbros (which are cumulates of Mauna Loa melts), this can be taken
209 as evidence for sulfide fractionation from Hawaiian magmas at depth as being the mechanism
210 generating the negative Pb anomalies in high (Sr/Ce)_N inclusions.

211 The ⁸⁷Sr/⁸⁶Sr of melt inclusions from the five lavas examined here (Table 1) are similar
212 to, or slightly larger, than the range observed for their respective host volcano. The ⁸⁷Sr/⁸⁶Sr
213 range for all of the Mauna Loa inclusions reported here is relatively small, ranging from
214 0.703700 to 0.703986 (⁸⁷Sr/⁸⁶Sr range of 406 ppm, Figure 5). The inclusions fall within the range
215 reported for Mauna Loa lavas (0.703599–0.703967; Hauri et al., 1996; Kurz et al., 1995). The
216 highest (Sr/Ce)_N melt inclusion (ML-2012-27_19b) has an ⁸⁷Sr/⁸⁶Sr of 0.703828 ± 0.000045, and
217 this inclusion, which also has the lowest (La/Sm)_N in this study, has indistinguishable ⁸⁷Sr/⁸⁶Sr
218 from the other Mauna Loa melt inclusions from the same lava (including Mauna Loa melt
219 inclusions with low (Sr/Ce)_N (Figure 6)). The Loihi melt inclusions (from two different lavas)
220 have ⁸⁷Sr/⁸⁶Sr ratios ranging from 0.70328 to 0.70367 (⁸⁷Sr/⁸⁶Sr range of 555 ppm), which
221 extends the range of ⁸⁷Sr/⁸⁶Sr identified for Loihi lavas (0.70344 to 0.70378; Bennett et al., 1996;
222 Garcia et al., 1995) to slightly lower ⁸⁷Sr/⁸⁶Sr. The Koolau melt inclusions (all from a single lava
223 sample) exhibit the largest range of ⁸⁷Sr/⁸⁶Sr among melt inclusions in this

Table 1. $^{87}\text{Sr}/^{86}\text{Sr}$ measurements made on melt inclusions and the glass of the host lava in this study.

Sample	Sr (ppm)	Ce (ppm)	(Sr/Ce) _n	Total Sr (ng)	[Sr] _{sample} /[Sr] _{blank}	$^{87}\text{Sr}/^{86}\text{Sr}^a$	2σ (std. err.)	ppm change in $^{87}\text{Sr}/^{86}\text{Sr}$ ratio from blank correction ^b
Mauna Loa - Pu'u Wahi (Puu2 & Puu7)								
Puu2-1-2	-	-	-	2.5	222	0.703772	0.000032	46
Puu2-1-9	270	20.6	1.11	15.5	292	0.703800	0.000021	35
Puu2-1-18a	337	26.7	1.06	2.8	53	0.703885	0.000049	191
Puu2-1-19	338	24.1	1.18	1.1	97	0.703899	0.000024	104
Puu2-1-39	215	15.8	1.14	7.3	1038	0.703935	0.000010	10
Puu7-1-20	438	24.9	1.48	1.2	177	0.703867	0.000034	57
Puu7-2-15	-	-	-	3.7	527	0.703845	0.000018	19
Puu7-2-92b	-	-	-	0.9	78	0.703917	0.000065	129
Puu7-2-80	324	20.3	1.34	9.2	817	0.703953	0.000016	12
Puu7-2-19	325	35.2	0.78	18.9	2690	0.703838	0.000008	4
Puu7-1-29	330	25.2	1.10	1.2	168	0.703804	0.000038	61
Puu7-3-19a	314	21.9	1.21	17.5	329	0.703916	0.000009	31
Puu7-3-31	265	19.1	1.16	28.8	542	0.703700	0.000023	19
Puu7-1-14	279	28.0	0.84	3.6	67	0.703947	0.000021	149
Puu7-1-30	325	31.6	0.87	2.5	46	0.703896	0.000013	218
Puu7-1-36	338	25.9	1.10	23.5	441	0.703770	0.000014	23
Puu7-2-62	334	24.3	1.16	3.1	444	0.703887	0.000030	23
Puu7-1-41	330	22.8	1.21	7.7	682	0.703977	0.000023	15
Puu7-2-6	327	25.8	1.07	9.8	1400	0.703811	0.000010	7
Puu7-2-40a	280	19.2	1.22	9.6	855	0.703770	0.000021	12
Puu7-2-42	336	22.9	1.24	5.3	469	0.703986	0.000029	21
Puu7-2-7a	311	22.5	1.16	3.1	445	0.703942	0.000040	23
Puu7-1-10	355	26.3	1.14	13.5	1923	0.703949	0.000008	5
Puu7-2-52	345	23.0	1.26	5.0	447	0.703882	0.000035	23
host glass^c	319	25.9	1.04			0.703912	0.000008	
Mauna Loa ML-2012-27								
ML-2012-27_2	283	15.3	1.56	10.0	1027	0.703881	0.000013	10
ML-2012-27_5a	457	38.1	1.01	10.2	1042	0.704010	0.000016	10
ML-2012-27_7	441	34.1	1.09	2.9	300	0.703887	0.000016	34
ML-2012-27_18a	426	35.8	1.00	0.7	69	0.704039	0.000030	144
ML-2012-27_21a	437	34.4	1.07	1.8	181	0.704009	0.000045	55
ML-2012-27_25	411	30.2	1.15	2.1	215	0.703985	0.000021	46
ML-2012-27_19b	786	9.1	7.24	1.4	74	0.703828	0.000045	137
host glass	344	27.6	1.05			0.703909	0.000006	
Koolau - K89-6								
K89-6_52	-	-	-	3.5	363	0.704401	0.000031	26
K89-6_53	260	16.2	1.35	0.5	25	0.703654	0.000079	416
K89-6_55	244	14.1	1.45	10.5	1495	0.703960	0.000027	7
K89-6_65	327	20.0	1.38	1.4	86	0.703864	0.000026	118
K89-6_76a	267	17.6	1.27	0.6	65	0.703906	0.000041	155
host glass	366	23.3	1.32			0.703965	0.000006	
Loihi - 6K490-1								
6K490-1_51	-	-	-	0.9	52	0.703284	0.000093	211
6K490-1_78	459	36.1	1.07	0.3	31	0.703665	0.000090	339
host glass	460	42.1	0.92			0.703586	0.000006	
Loihi - 6K490-2								
6K490-2_79a	507	44.5	0.96	1.1	63	0.703363	0.000033	173
host glass	412	35.0	0.99			0.703574	0.000006	

Note: The Sr and Ce fractionation-corrected concentrations are reported here, but not for partially crystalline inclusions.

^a $^{87}\text{Sr}/^{86}\text{Sr}$ values have been blank corrected and corrected for the offset between the preferred (0.710240) and the measured $^{87}\text{Sr}/^{86}\text{Sr}$ of NBS987.

^b The change in $^{87}\text{Sr}/^{86}\text{Sr}$ ratio due to the blank correction (ppm) is calculated as $(^{87}\text{Sr}/^{86}\text{Sr}_{\text{meas-norm987}} - ^{87}\text{Sr}/^{86}\text{Sr}_{\text{blank-corrected}}) / ^{87}\text{Sr}/^{86}\text{Sr}_{\text{meas-norm987}} * 10^6$.

^c Sr concentration and $^{87}\text{Sr}/^{86}\text{Sr}$ of Pu'u Wahi glass is from Reinhard et al. (2018).

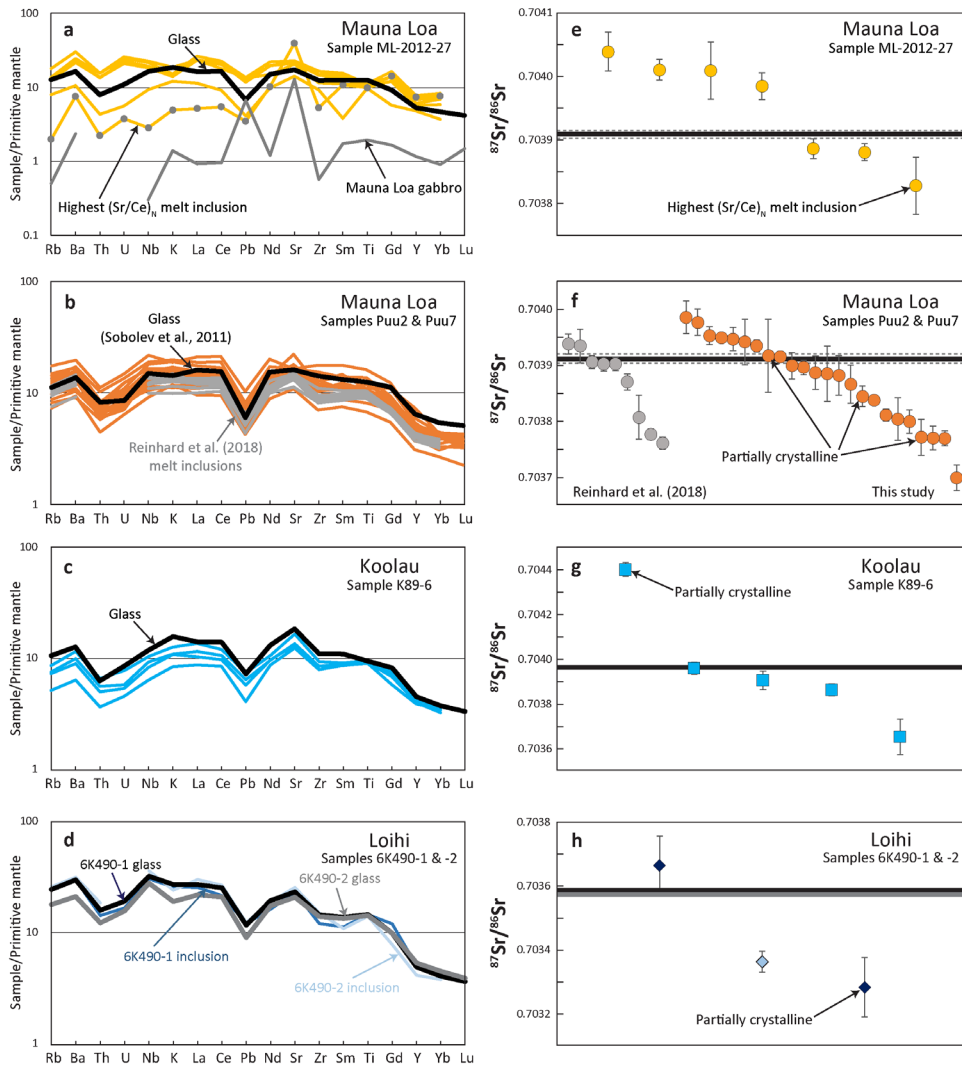


Figure 5. Primitive mantle normalized trace element patterns, or spidergrams, (left panels) and corresponding $^{87}\text{Sr}/^{86}\text{Sr}$ values (right panels) of all Hawaiian melt inclusions and host pillow/tephra glass in this study (note that 5 melt inclusions—Puu2-1-2, Puu7-2-15, Puu7-2-92b, K89-6_52, 6K490-1_51—are crystalline, so their spidergrams are not shown, but $^{87}\text{Sr}/^{86}\text{Sr}$ are). Concentrations shown in the figure have been corrected for addition or subtraction of equilibrium olivine so that the melt inclusions are in equilibrium with the host olivine. **(a–b)** Spidergrams for melt inclusions and host tephra from the three Mauna Loa samples—ML-2012-27 and the Pu'u Wahi samples (Puu2 and Puu7)—are shown together with a spidergram from a Mauna Loa gabbro with the highest $(\text{Sr}/\text{Ce})_N$ (sample 98-65 from Gaffney (2002)); spidergrams for melt inclusions from Pu'u Wahi from Reinhard et al. (2018) are also shown. The Pu'u Wahi tephra trace element concentrations are from Sobolev et al. (2011). **(c)** Spidergrams of Koolau melt inclusions from sample K89-6 with the host glass. **(d)** Spidergrams of Loihi melt inclusions from samples 6K490-1 and 6K490-2 are shown with the two respective host glasses. **(e–f)** The $^{87}\text{Sr}/^{86}\text{Sr}$ of the host pillow/tephra glass is shown as a straight line and dashed lines represent the 2σ (2SE) error bars. Panel **(f)** compares the $^{87}\text{Sr}/^{86}\text{Sr}$ of melt inclusions from Mauna Loa samples “Puu2” and “Puu7” analyzed here (orange symbols) and by Reinhard et al. (2018) (grey symbols). The $^{87}\text{Sr}/^{86}\text{Sr}$ results (generated in two different labs, UCSB and Vrije University, respectively) are remarkably consistent (the $^{87}\text{Sr}/^{86}\text{Sr}$ of the host tephra glass is shown as a straight line and was analyzed by Reinhard et al. (2018)). Partially crystalline inclusions are indicated in panels **(f–h)**, and spidergrams are not available for these inclusions. Note that the host pillow glass $^{87}\text{Sr}/^{86}\text{Sr}$ ratios for the two Loihi lavas—6K490-1 and 6K490-2—are indistinguishable in panel **(h)**.

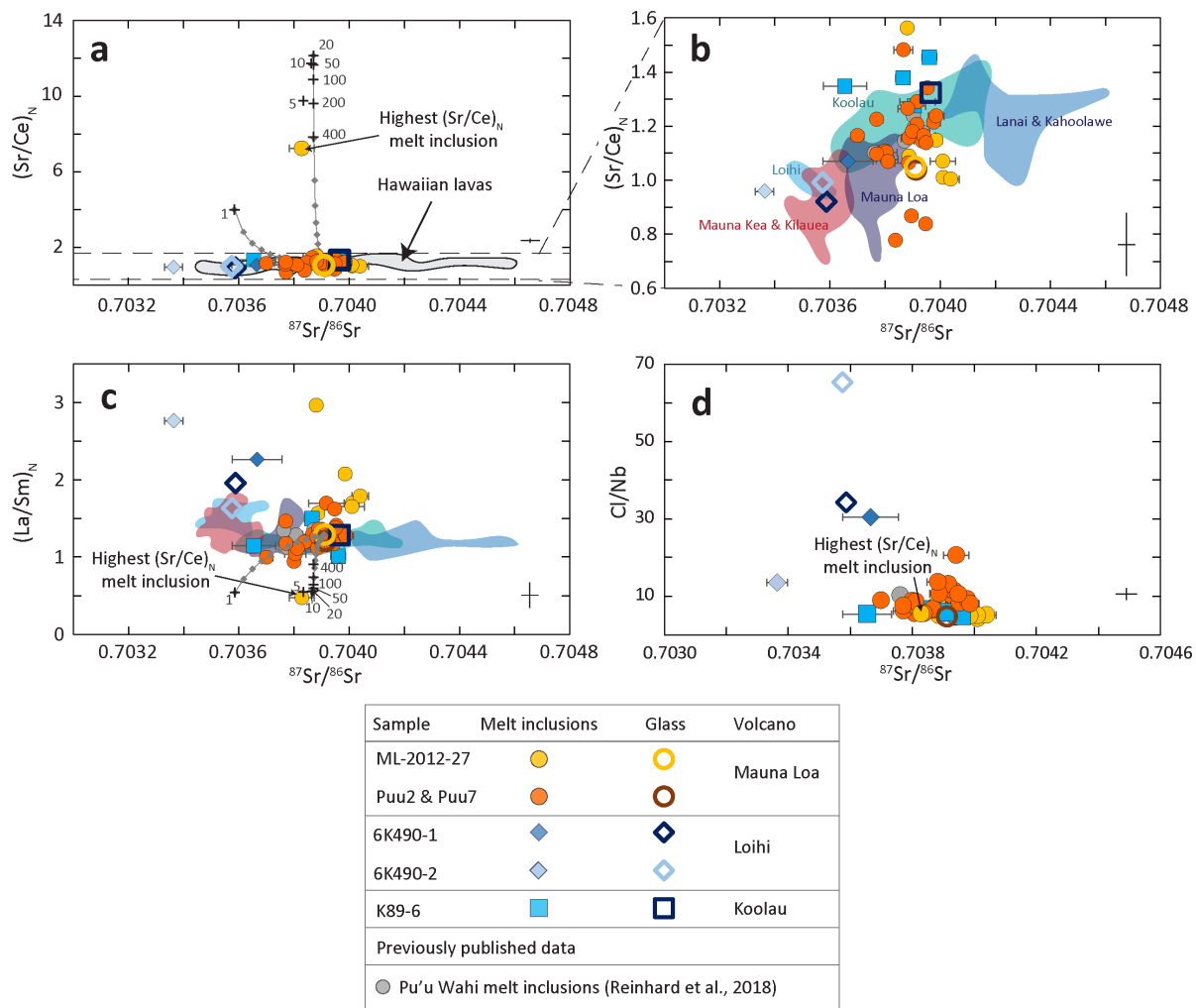


Figure 6. Important trace element ratios versus $^{87}\text{Sr}/^{86}\text{Sr}$. (a–b) $(\text{Sr}/\text{Ce})_N$ versus $^{87}\text{Sr}/^{86}\text{Sr}$. (c) $(\text{La}/\text{Sm})_N$ versus $^{87}\text{Sr}/^{86}\text{Sr}$. (d) Cl/Nb versus $^{87}\text{Sr}/^{86}\text{Sr}$. Note that melt inclusions in Sobolev et al. (2011) with $^{87}\text{Sr}/^{86}\text{Sr}$ are not shown as described in Section 3, and melt inclusions from Sobolev et al. (2000), including high $(\text{Sr}/\text{Ce})_N$ inclusions, do not have $^{87}\text{Sr}/^{86}\text{Sr}$. Fields for individual Hawaiian volcanoes are shown in (b) and (c) and the data are from Frey et al. (2016), which were filtered to exclude altered and differentiated lavas, as described in the Supplementary Methods Section S1.5, and thus the full range of $^{87}\text{Sr}/^{86}\text{Sr}$ for the volcanoes is not necessarily represented in this figure. Each plot on the left-hand side shows the diffusive interaction model results (black crosses) for Mauna Loa based on the Peterson et al. (2014) model and the numbers next to the crosses represent the number of years of diffusion. Mixing lines (grey lines with small grey diamonds representing increments of 10%) are shown between the ML-2012-27 host tephra composition and diffusion model results of 1 year and 20 years. For panel (d), note that samples ML-2012-27 and K89-6 do not have published Cl concentrations and Cl was not analyzed in the glasses in this study. Pu'u Wahi glass Cl concentration is from Sobolev et al. (2011). Cl concentrations for Loihi samples 6K490-1 and 6K490-2 are from Pietruszka et al. (2011). All panels show average 2σ error bars in the bottom right corner of plots.

227 study (0.703654 ± 0.000079 to 0.704401 ± 0.000031 , 1062 ppm total variability), which is
228 encompassed by the range of $^{87}\text{Sr}/^{86}\text{Sr}$ in Koolau lavas (0.703487 to 0.70451; Roden et al., 1994;
229 Tanaka et al., 2002). While there is $^{87}\text{Sr}/^{86}\text{Sr}$ heterogeneity in the Loihi and Koolau inclusions
230 examined here, the heterogeneity is not surprising given heterogeneity observed in olivine-hosted
231 melt inclusions at other OIB localities (Jackson & Hart, 2006; Harlou et al., 2009; Reinhard et
232 al., 2016, 2018). What is surprising is the remarkable $^{87}\text{Sr}/^{86}\text{Sr}$ homogeneity across the different
233 Mauna Loa melt inclusions examined here, in spite of extreme trace element variability (e.g.,
234 $(\text{Sr}/\text{Ce})_{\text{N}}$). Below we focus the discussion on this unusual $^{87}\text{Sr}/^{86}\text{Sr}$ homogeneity.

235 Loihi melt inclusions have higher Cl contents (319 to 606 ppm) than the melt inclusions
236 from Mauna Loa (measured concentration of 10 to 183 ppm; see Table S1) or Koolau (20 to 45
237 ppm) (Figure 6e). Elevated Cl in Loihi melts was observed previously (Kent et al., 1999a, 1999b,
238 2002). Similarly, the three Loihi inclusions have the largest range in Cl/Nb (14 to 30), consistent
239 with the high Cl concentrations observed in Loihi glasses (Kent et al., 1999a, 1999b, 2002). In
240 comparison, Cl/Nb ratios tend to lower values in Koolau melt inclusions (5 to 7) and Mauna Loa
241 inclusions (4 to 14, excluding a single melt inclusion, sample Puu7-2-7a, with Cl/Nb = 21).
242 Critically, $^{87}\text{Sr}/^{86}\text{Sr}$ does not covary with Cl/Nb in the melt inclusion suite examined here,
243 suggesting seawater-derived materials are not responsible for generating the $^{87}\text{Sr}/^{86}\text{Sr}$
244 heterogeneity (see Sections 4.1 and 4.3 for discussion on the interpretation).

245 Melt inclusions from Pu'u Wahi were previously analyzed for $^{87}\text{Sr}/^{86}\text{Sr}$ by Sobolev et al.
246 (2011) and Reinhard et al. (2018). Sobolev et al. (2011) analyzed a suite of 137 inclusions from
247 Pu'u Wahi using a laser ablation (LA) single-collector ICP-MS technique and reported an
248 extraordinary range in $^{87}\text{Sr}/^{86}\text{Sr}$, from 0.7021 to 0.7081 (which is a range of ~8500 ppm, or
249 approximately ± 3000 ppm 2σ relative standard deviation, or 2RSD; Figure 7). They showed that
250 the two UDMs identified in Pu'u Wahi inclusions yield the most extreme high $^{87}\text{Sr}/^{86}\text{Sr}$ values
251 (0.7081 ± 0.0004 ; two melt inclusions analyzed at least ten times each), and if these UDM
252 inclusions are excluded, the $^{87}\text{Sr}/^{86}\text{Sr}$ in their dataset has an average of 0.7039 ± 0.0019 (2SD)
253 (approximately ± 2700 ppm 2RSD). In contrast, the 33 Pu'u Wahi melt inclusions analyzed for
254 $^{87}\text{Sr}/^{86}\text{Sr}$ by TIMS in this study and the study of Reinhard et al. (2018) show very little variability
255 (i.e., 0.703700 to 0.703986, or approximately ± 200 ppm 2RSD across both TIMS studies). Like
256 Reinhard et al. (2018), we did not identify UDM inclusions, which may partially explain the lack
257 of extreme $^{87}\text{Sr}/^{86}\text{Sr}$ in our study (but see below). However, even if the two UDM inclusions are
258 excluded from the Sobolev et al. (2011) dataset, the 2RSD in $^{87}\text{Sr}/^{86}\text{Sr}$ of the remaining 135
259 inclusions (i.e., approximately ± 2700 ppm) is still ~13 times greater than the combined 2RSD in
260 $^{87}\text{Sr}/^{86}\text{Sr}$ identified in this study and the study of Reinhard et al. (2018) (i.e., approximately ± 200
261 ppm).

262 In summary, the TIMS $^{87}\text{Sr}/^{86}\text{Sr}$ results for Pu'u Wahi inclusions from two different
263 labs—Vrije University ($N = 9$ inclusions; Reinhard et al., 2018) and UCSB ($N = 24$ inclusions;
264 this study)—are in close agreement, but disagree substantially with the reported $^{87}\text{Sr}/^{86}\text{Sr}$
265 variability in Pu'u Wahi inclusions from Sobolev et al. (2011) (Figure 7). One explanation is that
266 there is an inherent difference in precision between the two techniques. Rubidium (as well as

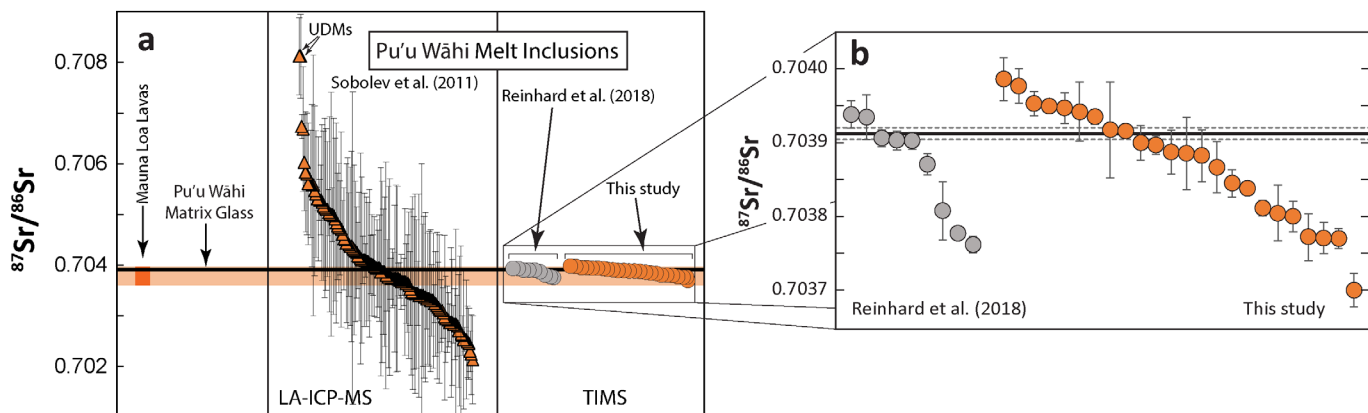


Figure 7. $^{87}\text{Sr}/^{86}\text{Sr}$ of Mauna Loa Pu'u Wahi melt inclusions by two different methods. **(a)** The $^{87}\text{Sr}/^{86}\text{Sr}$ of Pu'u Wahi melt inclusions measured by LA-ICP-MS (Sobolev et al., 2011) and TIMS (Reinhard et al., 2018; this study) are compared to the $^{87}\text{Sr}/^{86}\text{Sr}$ range of Mauna Loa lavas (orange bar = 0.703599–0.703967; Hauri et al., 1996; Kurz et al., 1995) and of the Pu'u Wahi glass (horizontal black line; Reinhard et al., 2018). The ultra-depleted melt (UDM) inclusions from Sobolev et al. (2011) are marked separately. Even when the UDM inclusions are excluded, the 2RSD in $^{87}\text{Sr}/^{86}\text{Sr}$ of the Pu'u Wahi melt inclusions determined by LA-ICP-MS greatly exceeds (by a factor of 13) the 2RSD determined by TIMS. Panel **(b)** shows only the $^{87}\text{Sr}/^{86}\text{Sr}$ of Pu'u Wahi melt inclusions analyzed by TIMS compared to the Pu'u Wahi matrix glass (horizontal black line with 2SE represented by the dashed lines) analyzed by Reinhard et al. (2018).

267 other isobaric interferences, e.g., ^{84}Kr , ^{86}Kr) limits the precision of $^{87}\text{Sr}/^{86}\text{Sr}$ analyses performed
 268 by LA-ICP-MS, whereas chemical separation of Sr provides a means to minimize Rb prior to
 269 analysis by TIMS, and TIMS does not suffer from the other isobaric interferences from the
 270 carrier gas. We suggest that the difference in Pu'u Wahi melt inclusion $^{87}\text{Sr}/^{86}\text{Sr}$ variability
 271 determined by LA single-collector ICP-MS (Sobolev et al., 2011) and TIMS (this study;
 272 Reinhard et al., 2018) is the result of the former technique generating lower-precision analyses of
 273 a relatively-homogeneous melt inclusion population (i.e., a population with $^{87}\text{Sr}/^{86}\text{Sr}$ variability
 274 similar to that identified by TIMS). To test this hypothesis, we calculate the average $^{87}\text{Sr}/^{86}\text{Sr}$ and
 275 2SD of the Pu'u Wahi melt inclusions analyzed by the LA-ICP-MS technique, and compare this

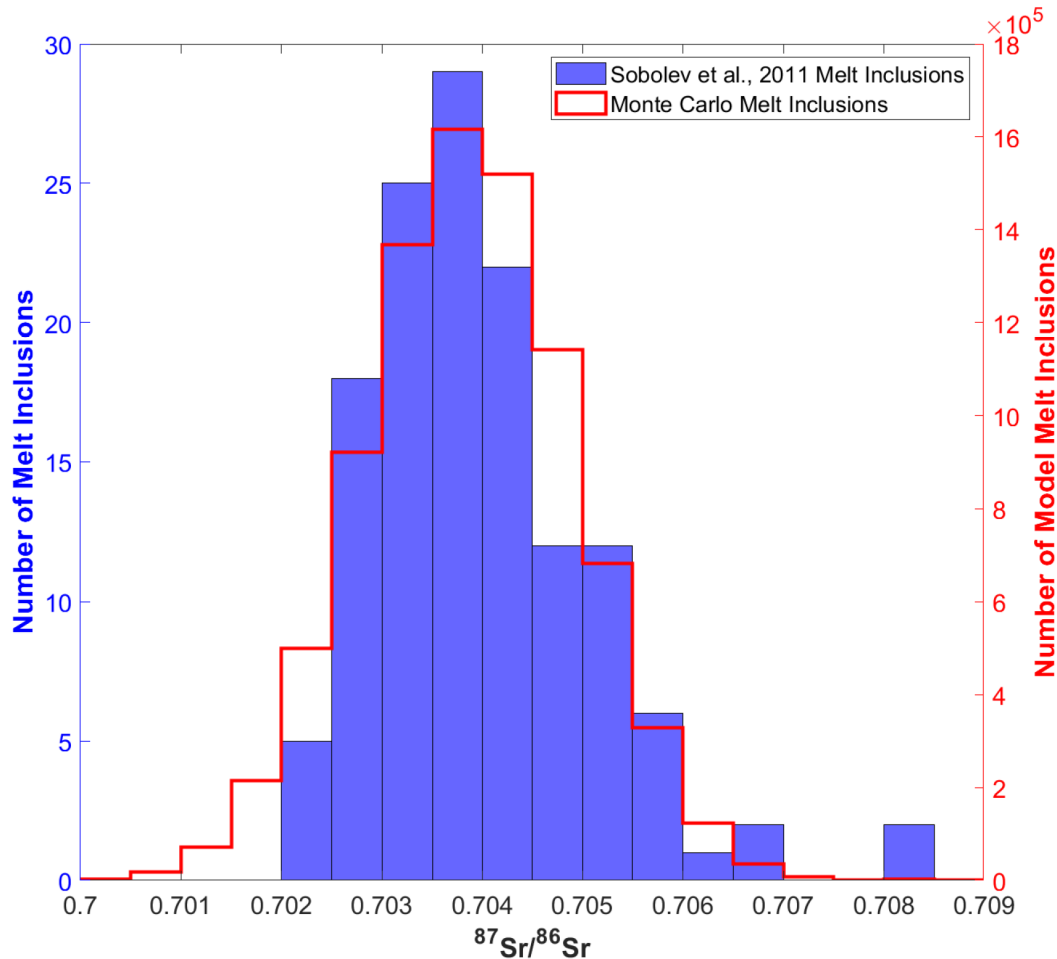


Figure 8. The red histogram displays the resulting model variability in $^{87}\text{Sr}/^{86}\text{Sr}$ if a relatively homogeneous population (i.e., $^{87}\text{Sr}/^{86}\text{Sr}$ variability is approximately ± 200 ppm, 2RSD) of melt inclusions, like that found by the TIMS studies of Pu'u Wahi melt inclusions (Reinhard et al., 2018; this study), is modelled using a Monte Carlo method that assigns the melt inclusions larger uncertainties from the distribution of measurement uncertainties associated with the Sobolev et al. (2011) ICP-MS analyses. The red histogram represents the $^{87}\text{Sr}/^{86}\text{Sr}$ of model melt inclusions resulting from 10^6 iterations of the Monte Carlo simulation. The $^{87}\text{Sr}/^{86}\text{Sr}$ values of the Pu'u Wahi melt inclusions reported by Sobolev et al. (2011) are shown as a blue histogram). In summary, larger measurement uncertainties associated with a relatively homogeneous population of melt inclusions can generate apparent heterogeneity that mimics the extreme $^{87}\text{Sr}/^{86}\text{Sr}$ heterogeneity reported in the Puu Wahi inclusions by the Sobolev et al. (2011).

276 to the average $^{87}\text{Sr}/^{86}\text{Sr}$ and 2SD of the Pu'u Wahi melt inclusions analyzed by TIMS. The
 277 average of Sobolev et al.'s (2011) $^{87}\text{Sr}/^{86}\text{Sr}$ measurements is 0.7040 ± 0.0021 (2SD, $N = 137$)
 278 (with the two UDM inclusions), or 0.7039 ± 0.0019 (2SD, $N = 135$) (without the two UDM
 279 inclusions). These average $^{87}\text{Sr}/^{86}\text{Sr}$ values are indistinguishable from the average $^{87}\text{Sr}/^{86}\text{Sr}$
 280 obtained on Pu'u Wahi melt inclusions at the Vrije University TIMS lab (0.703867 ± 0.00013 ,
 281 2SD, $N = 9$) and the average $^{87}\text{Sr}/^{86}\text{Sr}$ of melt inclusions from the UCSB TIMS lab reported here
 282 (0.703873 ± 0.000152 , 2SD, $N = 24$), which are also indistinguishable from the Pu'u Wahi tephra
 283 glass $^{87}\text{Sr}/^{86}\text{Sr}$ (0.703912 ± 0.000008 , 2SE) and the range in $^{87}\text{Sr}/^{86}\text{Sr}$ reported in Mauna Loa
 284 whole rocks (0.70360 to 0.703967 ; Hauri et al., 1996; Kurz et al., 1995). This result is consistent

285 with the hypothesis that the disagreement between the TIMS $^{87}\text{Sr}/^{86}\text{Sr}$ analyses and the LA-ICP-
286 MS $^{87}\text{Sr}/^{86}\text{Sr}$ analyses are a result of the significantly larger errors associated with the Sobolev et
287 al. (2011) $^{87}\text{Sr}/^{86}\text{Sr}$ measurements.

288 In order to further test the influence of measurement reproducibility on the total observed
289 $^{87}\text{Sr}/^{86}\text{Sr}$ variability in the Pu'u Wahi melt inclusion suite, we performed a Monte Carlo
290 simulation. This Monte Carlo simulation (Figure 8) evaluates the $^{87}\text{Sr}/^{86}\text{Sr}$ variability in Pu'u
291 Wahi melt inclusions that would result if a relatively homogeneous population of Pu'u Wahi
292 melt inclusions (like that found by the TIMS studies) is assigned the larger measurement
293 uncertainties associated with the Sobolev et al. (2011) single-collector ICP-MS method. In the
294 simulation, we first calculate an uncertainty equal to the average 2SD of the 135 Pu'u Wahi melt
295 inclusion measurements (i.e., including only the melt inclusions with at least one replicate
296 analysis) reported by Sobolev et al. (2011), which is ± 2919 ppm. This is used to generate a
297 Gaussian distribution, which has a 2RSD of ± 2919 ppm, and from this distribution values are
298 drawn randomly in each iteration of the model and then assigned as errors to each of the 33 Pu'u
299 Wahi melt inclusions analyzed by TIMS in this study and Reinhard et al. (2018). The range of
300 $^{87}\text{Sr}/^{86}\text{Sr}$ in the 33 melt inclusions in the model is then calculated, and this process was then
301 repeated 10^6 times. This simulation yields a range in $^{87}\text{Sr}/^{86}\text{Sr}$ for each of a million different
302 model melt inclusion populations, giving a 95% confidence interval of ~ 8200 ppm for the ranges
303 in $^{87}\text{Sr}/^{86}\text{Sr}$ across all simulations. The 95% confidence interval in the range in $^{87}\text{Sr}/^{86}\text{Sr}$ for the
304 simulation approaches the ~ 8500 ppm range in $^{87}\text{Sr}/^{86}\text{Sr}$ reported in the suite of 135 melt
305 inclusions analyzed by Sobolev et al. (2011), and the comparison is shown in Figure 8. In
306 summary, if the larger measurement errors of Sobolev et al. (2011) data are applied to a
307 relatively homogeneous population of melt inclusions analyzed by TIMS, it is possible to
308 generate *apparent* $^{87}\text{Sr}/^{86}\text{Sr}$ variability that is comparable to the reported $^{87}\text{Sr}/^{86}\text{Sr}$ variability in
309 Sobolev et al. (2011). Thus, the large reported $^{87}\text{Sr}/^{86}\text{Sr}$ variability previously found in Pu'u Wahi
310 melt inclusions appears to be the result of larger uncertainties associated with the $^{87}\text{Sr}/^{86}\text{Sr}$
311 analyses by ICP-MS.

312 We did not encounter any melt inclusions with the UDM trace element patterns identified
313 by Sobolev et al. (2011). Therefore, we acknowledge that these UDM melt inclusions could have
314 different $^{87}\text{Sr}/^{86}\text{Sr}$ compositions than the Pu'u Wahi inclusions that we examine here. However,
315 we note that the high $^{87}\text{Sr}/^{86}\text{Sr}$ values (~ 0.708) reported in the UDM inclusions are generated in
316 our Monte Carlo simulation, which can be seen in Figure 8 by the overlap of the model melt
317 inclusions in red with the Sobolev et al. (2011) melt inclusions in blue at ~ 0.708 . Therefore, the
318 $^{87}\text{Sr}/^{86}\text{Sr}$ data for Pu'u Wahi melt inclusions from Sobolev et al. (2011) are not included in Figure
319 6 or in the interpretation of Mauna Loa $^{87}\text{Sr}/^{86}\text{Sr}$ data, but we do show the Sobolev et al. (2011)
320 melt inclusions $^{87}\text{Sr}/^{86}\text{Sr}$ data in comparison to the TIMS data in Figure 7. Below we address
321 only the origin of the non-UDM inclusions with high $(\text{Sr}/\text{Ce})_N$ identified by Sobolev et al. (2000,
322 2011), which were argued by Sobolev et al. (2000) to be sourced by ancient recycled gabbro.

323 4. Discussion

324 4.1 Processes that can influence melt inclusion compositions prior to, and following, 325 entrapment.

326 When working with melt inclusions, it is necessary to consider how the melts may have
327 been modified before and after entrapment. For example, following entrapment, melt inclusion
328 compositions can be affected by diffusive exchange, through the host crystal, with the

329 surrounding melt. Relative to Hawaiian lavas, and host glasses, the melt inclusions in this study
 330 tend to have lower FeO_t (Figure S4), which is indicative of diffusive Fe-Mg exchange between
 331 the melt inclusion and the host melt. Fe-Mg diffusive exchange in melt inclusions is relatively
 332 common, and has been attributed to slower cooling, as a longer residence time is required for Fe
 333 to diffuse out of the host mineral (e.g., Danyushevsky et al., 2000; Gaetani & Watson, 2000;
 334 Sobolev & Danyushevsky, 1994). However, Fe-Mg exchange does not influence trace element
 335 ratios or the $^{87}\text{Sr}/^{86}\text{Sr}$ of the melt inclusion, therefore “Fe loss” does not affect the conclusions of
 336 this study and we do not attempt to correct for it.

337 Additionally, melt inclusions experience post-entrapment crystallization during cooling,
 338 and we correct for post-entrapment loss of olivine to the melt inclusion wall. All Hawaiian melt
 339 inclusion major and trace element data shown in the figures have been fractionation corrected to
 340 be in equilibrium with the forsterite (Fo) content of the host olivine by adding or subtracting
 341 equilibrium olivine at 0.1% increments. For the calculation, we assume (i) an olivine-melt Fe-Mg
 342 K_d of 0.30 (Ford et al., 1983; $K_d = (\text{Fe}^{2+}/\text{Mg})_{\text{olivine}} / (\text{Fe}^{2+}/\text{Mg})_{\text{melt}}$) and (ii) 10% of the total iron in
 343 the melt is Fe^{3+} (following Hauri, 1996). Major, volatile, and trace element concentrations
 344 corrected for olivine addition or subtraction are shown in Table S1, together with measured
 345 concentrations.

346 Prior to entrapment, melts can assimilate altered oceanic crust. Chlorine is an indicator
 347 for assimilation of seawater-derived materials, including altered oceanic crust. Thus, melts that
 348 have assimilated seawater-derived materials can have elevated Cl, Cl/ K_2O , and Cl/Nb ratios
 349 (Jambon et al., 1995; Kendrick et al., 2013a, 2015; Kent et al., 1999a, 1999b, 2002; Koleszar et
 350 al., 2009; Lassiter et al., 2002; Michael & Cornell, 1998). Chlorine is fluid mobile (e.g., Debret
 351 et al., 2014; John et al., 2011; Kendrick et al., 2013b; Rose-Koga et al., 2012; Straub & Layne,
 352 2003), therefore recycled oceanic crust that has gone through a subduction filter is not predicted
 353 to retain high Cl/ K_2O and Cl/Nb ratios (e.g., Kendrick et al., 2013a, 2015, 2017; Rowe &
 354 Lassiter, 2009). Mantle-derived lavas have low Cl/Nb ratios relative to lavas influenced by
 355 assimilation of altered oceanic crust (e.g., 5–17; Michael & Cornell, 1998; Rowe & Lassiter,
 356 2009; Rowe et al., 2015; Saal et al., 2002; Stroncik & Haase, 2004). The Hawaiian melt
 357 inclusions considered here generally have mantle-like Cl/Nb (ratios of 4 to 14, but inclusion
 358 Puu7-2-7a has a higher ratio, 21), except for Loihi glasses (ratios of 34 to 65) and their melt
 359 inclusions (ratios of 14 to 30), which confirms observations of elevated Cl and Cl/Nb in Loihi
 360 glasses and melt inclusions (Kent et al., 1999a, 1999b). Critically for this study, the highest
 361 $(\text{Sr}/\text{Ce})_N$ melt inclusion has mantle-like Cl/Nb, so assimilation of shallow-level altered oceanic
 362 crust is unlikely to be involved in its origin. However, the low Cl/Nb ratio of the high $(\text{Sr}/\text{Ce})_N$
 363 inclusion does not exclude a contribution from the Cretaceous lower (gabbroic) oceanic crust
 364 beneath Hawai'i (which may have mantle-like Cl/Nb, see Section 4.2), which is discussed below.
 365 None of the high Cl/Nb inclusions (i.e., Loihi) have elevated $(\text{Sr}/\text{Ce})_N$.

366 **4.2 Source of high $(\text{Sr}/\text{Ce})_N$ “ghost plagioclase” in Mauna Loa melt inclusions: bulk** 367 **assimilation of gabbro?**

368 This study presents the highest magmatic $(\text{Sr}/\text{Ce})_N$ ratio in Hawaiian melts measured to
 369 date, suggesting a role for a plagioclase-bearing lithology, such as cumulate gabbro, in the
 370 petrogenesis of this, and similar, high $(\text{Sr}/\text{Ce})_N$ inclusions from Hawai'i. However, the
 371 mechanism for the incorporation of the high $(\text{Sr}/\text{Ce})_N$ “ghost plagioclase” signature (i.e., elevated
 372 $(\text{Sr}/\text{Ce})_N$ without concomitant enrichment in Al_2O_3) remains controversial (Peterson et al., 2014;
 373 Saal et al., 2007; Sobolev et al., 2000; Yaxley & Sobolev, 2007).

374 Gabbros from the deeper regions of Mauna Loa volcano may have mantle-like Cl/Nb, so
 375 assimilation of such gabbros may not be detected with Cl/Nb. In order to test for direct gabbro
 376 assimilation, we present a mixing model between the average “normal” Pu'u Wahi melt inclusion
 377 composition (an average composition of Pu'u Wahi melt inclusions lacking anomalous major and
 378 trace elements signatures, defined in Table S10) and the Mauna Loa gabbroic xenolith with the
 379 highest $(\text{Sr}/\text{Ce})_N$ —to minimize the quantity of gabbro needed to generate the elevated $(\text{Sr}/\text{Ce})_N$ in
 380 the melt inclusion—from Gaffney (2002; Figure 3). The highest $(\text{Sr}/\text{Ce})_N$ melt inclusion (sample
 381 ML-2012-27_19b) is offset from the normal melt inclusion-Mauna Loa gabbro mixing line to
 382 lower Al_2O_3 at a given $(\text{Sr}/\text{Ce})_N$, and is therefore not well described by assimilation of this or any
 383 other available Mauna Loa gabbro composition. Additionally, the mixing line in Figure 3a
 384 informs the minimum amount of Mauna Loa gabbro assimilation (90%) required to generate the
 385 high $(\text{Sr}/\text{Ce})_N$ in this melt inclusion, given available gabbro compositions at Mauna Loa. This
 386 high proportion of Mauna Loa gabbro is also inconsistent with the same mixing model in Al_2O_3
 387 versus MgO space (Figure 3c): This is because 90% Mauna Loa gabbro assimilation by the
 388 inclusion would cause it to plot off (toward higher Al_2O_3) of the array formed by Hawaiian lavas
 389 in Al_2O_3 versus MgO space, but the high $(\text{Sr}/\text{Ce})_N$ inclusion is not displaced from this array
 390 (Figure 3c).

391 Assimilation of gabbro from the Cretaceous oceanic crust that underlies Hawai'i was also
 392 tested using Gabal Gerf ophiolite gabbros (Zimmer et al., 1995), which serve as a proxy for
 393 Cretaceous oceanic crust gabbro. However, there is no mixing model between normal-type Pu'u
 394 Wahi melts and Gabal Gerf gabbros that can account for the ghost plagioclase inclusion (one
 395 mixing line is shown, which trends to the highest $(\text{Sr}/\text{Ce})_N$ Gabal Gerf composition, in Figure 3).
 396 The mixing lines generate Al_2O_3 that is too high for the high $(\text{Sr}/\text{Ce})_N$ inclusion in $(\text{Sr}/\text{Ce})_N$
 397 versus Al_2O_3 and Al_2O_3 versus MgO space. Thus, we can exclude bulk assimilation of gabbro in
 398 the genesis of the high $(\text{Sr}/\text{Ce})_N$ melt inclusion. This observation is central to the paradox of the
 399 “ghost plagioclase” signature, where trace element signatures (i.e., high $(\text{Sr}/\text{Ce})_N$) indicate
 400 gabbroic influence, whereas major elements (i.e., Al_2O_3) are inconsistent with direct assimilation
 401 of gabbro. While we can exclude direct assimilation of gabbro, these mixing models do not
 402 address the two remaining hypotheses for the origin of high $(\text{Sr}/\text{Ce})_N$ signatures at hotspots—
 403 ancient recycled gabbro or diffusive interaction between Hawaiian melts and Mauna Loa
 404 gabbros—which we test with Sr isotopes below.

405 406 **4.3 Source of high $(\text{Sr}/\text{Ce})_N$ “ghost plagioclase” in Mauna Loa melt inclusions: diffusive** 407 **exchange between upwelling melts and shallow gabbro?**

408
409 Examining lavas and melt inclusions from the Galapagos that exhibit the trace element
 410 signature commonly associated with plagioclase, Saal et al. (2007) and Peterson et al. (2014)
 411 argue against the presence of ancient recycled oceanic gabbro in the mantle source. Instead, they
 412 proposed that diffusive exchange between mantle-derived melts and gabbros in the deep volcanic
 413 sections of Galapagos volcanoes generate the measured, plagioclase-related (i.e., high $(\text{Sr}/\text{Ce})_N$)
 414 trace element signatures. In addition to melts with plagioclase-influenced compositions,
 415 Galapagos olivine-hosted melt inclusions from Fernandina exhibit the ghost plagioclase
 416 signature. Peterson et al. (2014) examined the range of trace element and Pb isotopic
 417 compositions that could be generated from both melting an ancient recycled oceanic gabbro in
 418 the deep mantle and from diffusive interaction in the shallow crust. Peterson et al. (2014)
 419 demonstrated that the recycled oceanic gabbro model cannot reproduce the trace element

420 signature and the Pb isotope compositions of the ghost plagioclase inclusions simultaneously.
421 However, the diffusive exchange model generates both the trace element and Pb isotope
422 compositions of the high (Sr/Ce)_N inclusions with the ghost plagioclase signature.

423 Therefore, instead of reflecting a source signature related to recycled gabbro
424 heterogeneities embedded in the plume, as advocated by Sobolev et al. (2000) for Hawai'i, the
425 model for the generation of ghost plagioclase signatures proposed by Saal et al. (2007) and
426 Peterson et al. (2014) suggests that it is a shallow process, where diffusive interaction between
427 plagioclase in lithospheric gabbros and upwelling hotspot melts results in the hotspot melts
428 inheriting high (Sr/Ce)_N signatures. In this diffusive exchange model, Sr diffuses through the
429 crustal plagioclase toward the upwelling plume melt because it has a higher diffusivity in
430 plagioclase relative to other trace elements, such as La and Nd. In this way, a large positive Sr
431 anomaly can be inherited by the upwelling plume melt due to diffusive interaction with the
432 plagioclase, thereby generating the ghost plagioclase composition.

433 We apply the Peterson et al. (2014) “diffusive exchange” approach used in the Galapagos
434 to evaluate whether melt-gabbro diffusive interaction can generate the elevated (Sr/Ce)_N
435 signatures in Mauna Loa inclusions. The model parameters follow Peterson et al. (2014), except
436 that a Mauna Loa lava (sample J2-15-13, with a relatively high Sr content of 689 ppm; Wanless
437 et al., 2006) is used instead of the high-Sr concentration Galapagos melt used in Peterson et al.
438 (2014), and we track the influence of the diffusive exchange model on ⁸⁷Sr/⁸⁶Sr instead of Pb
439 isotopes. (An incompatible element rich melt, like J2-15-13 used here, may have been more
440 common during the pre-shield alkali volcanism at Mauna Loa.) A plagioclase trace element
441 composition is calculated that is in equilibrium with Mauna Loa lava J2-15-13 using a
442 plagioclase An₈₀ composition at 1200 °C and plagioclase-melt partition coefficients from Bédard
443 (2006). Hawaiian melt inclusions with ghost plagioclase signatures (similar to Galapagos melt
444 inclusions with ghost plagioclase signatures) are depleted in incompatible trace elements, except
445 those associated with plagioclase, which is reflected in the low (La/Sm)_N of the ghost plagioclase
446 inclusions. Because of this depleted nature, we use a 12% aggregated fractional melt of
447 Workman and Hart’s (2005) depleted MORB mantle (DMM) as the percolating melt that
448 diffusively exchanges with the plagioclase-rich lithology. The average of East Pacific Rise ridge
449 segments from Gale et al. (2013) is used for the initial ⁸⁷Sr/⁸⁶Sr composition of the percolating
450 melt. This percolating melt undergoes diffusive exchange with a troctolite (for simplicity)
451 hosting 50% modal plagioclase with the modeled trace element composition, where diffusive
452 exchange uses published trace element diffusivities (Cherniak, 1995, 2002, 2003; Cherniak &
453 Watson, 1994; Giletti & Casserly, 1994; Giletti & Shanahan, 1997) at 1200°C (see Table 2 for
454 diffusivities used). Hawaiian lava temperatures approach 1200°C (Gansecki et al., 2019), making
455 this an appropriate temperature for model calculation. The duration of diffusive interaction varies
456 from 1 year to 400 years in our model, as plagioclase trace element signatures are inherited by
457 the percolating melt as a function of time (Table 2). Because Sr has a higher diffusivity than Ce
458 and Al in plagioclase, the percolating DMM melt can inherit high (Sr/Ce)_N, but not elevated
459 Al₂O₃, thereby providing an explanation for the ghost plagioclase signature without invoking
460 direct gabbro assimilation (Danyushevsky et al., 2003) or ancient recycled gabbro (Sobolev et al.
461 2000). Depletion in light REEs relative to middle REEs is an outcome of the diffusive exchange
462 model, where lower (La/Sm)_N are generated as higher (Sr/Ce)_N are produced (Figure 4). Finally,
463 we mix the diffusively modified melts with the host glass associated with the highest (Sr/Ce)_N
464 inclusion, sample ML-2012-27 (though mixing with average Pu'u Wahi normal-type melt
465 inclusions would not change the result), and then compare the mixtures to measured Hawaiian

466 melt inclusion compositions. Following 1 to 5 years of diffusive exchange (i.e., timescales that
 467 are well within crystal residence times in Hawaiian magmas; e.g., Cooper et al., 2001; Vinet &
 468 Higgins, 2010; Wieser et al., 2019), the $(\text{La}/\text{Sm})_{\text{N}}$, $(\text{Sr}/\text{Ce})_{\text{N}}$, and $^{87}\text{Sr}/^{86}\text{Sr}$ composition of the
 469 highest Mauna Loa $(\text{Sr}/\text{Ce})_{\text{N}}$ inclusion is matched in the diffusive exchange model.

470 This model requires the presence of Mauna Loa gabbros deep in the volcanic pile of the
 471 volcano. Gaffney (2002) examined a suite of Mauna Loa gabbros (crystallized from Mauna Loa
 472 magmas), which provide evidence of cumulus plagioclase in the deep stratigraphy of the
 473 volcano. Although gabbroic xenoliths from Mauna Loa are uncommon, the lava pile is many
 474 kilometers thick, and only a fraction of the lava pile has been sampled directly. Therefore,
 475 gabbro could be more abundant in the deep shield than is suggested by the low abundance of
 476 gabbroic xenoliths that have been transported to the surface.

Table 2. Model parameters and output data for the diffusive interaction model based on the model of Peterson et al. (2014).

	$K_{\text{d}}(\text{plag-melt})^{\text{a}}$	$D_{\text{plag}}(1200^{\circ}\text{C},$ $\text{m}^2 \text{ s}^{-1})^{\text{b}}$	Plagioclase melt ^c	Initial melt ^d	Output data (concentrations in ppm)							
					(ppm)	(ppm)	1 year	5 years	10 years	20 years	50 years	100 years
Ba	0.230	8.09E-19	198	4.69	4.86	5.52	6.35	7.99	12.82	20.57	35.03	60.18
Th	0.050	3.10E-21	1.37	0.07	0.07	0.07	0.07	0.07	0.07	0.07	0.07	0.07
U	0.024	3.10E-21	0.47	0.03	0.03	0.03	0.03	0.03	0.03	0.03	0.03	0.03
Nb	0.030	3.10E-21	20.4	1.24	1.24	1.24	1.24	1.24	1.24	1.24	1.24	1.24
K	0.171	4.38E-16	7222	408	2364	5618	6368	6491	6494	6494	6494	6494
La	0.106	3.87E-19	21	1.60	1.60	1.62	1.64	1.67	1.78	1.96	2.32	3.01
Ce	0.081	3.87E-19	53.5	4.57	4.58	4.61	4.64	4.71	4.92	5.28	5.97	7.32
Pb	0.511	1.41E-17	1.69	0.15	0.23	0.52	0.80	1.17	1.55	1.63	1.63	1.63
Nd	0.084	2.92E-19	36	4.76	4.77	4.78	4.80	4.83	4.94	5.11	5.46	6.14
Sr	1.813	3.37E-17	689	63.5	217	534	647	680	682	682	682	682
Zr	0.004	3.10E-21	264	41.5	41.5	41.5	41.5	41.5	41.5	41.5	41.5	41.5
Hf	0.015	3.10E-21	6.33	1.27	1.27	1.27	1.27	1.27	1.27	1.27	1.27	1.27
Sm	0.056	2.92E-19	9.3	1.88	1.88	1.88	1.88	1.89	1.90	1.93	1.99	2.10
Eu	0.534	2.92E-19	3.06	0.74	0.83	1.13	1.39	1.67	1.88	1.94	2.01	2.15
Ti	0.076	3.10E-21	21049	5310	5310	5311	5311	5311	5312	5314	5317	5317
Dy	0.019	3.24E-19	6.77	3.37	3.58	3.58	3.58	3.58	3.58	3.58	3.58	3.58
Yb	0.015	5.06E-19	2.09	2.04	2.04	2.04	2.04	2.04	2.04	2.04	2.04	2.04
$^{87}\text{Sr}/^{86}\text{Sr}$			0.703872	0.702569	0.703585	0.703833	0.703863	0.703870	0.703871	0.703871	0.703871	0.703871

For the diffusion model we assume that the plagioclase grain size is 0.001 m, there is 1% melt, and 50% of the solid is plagioclase.

^aBédard (2006) for plagioclase of An_{50} at 1200°C

^bDiffusion coefficients for plagioclase at 1200°C from Cherniak and Watson (1994), Giletti and Casserly (1994), Cherniak (1995, 2002, 2003) and Giletti and Shanahan (1997). However, some trace elements do not have experimentally determined diffusion coefficients. For trace elements without this data, Peterson et al. (2014) estimated based on cation size and charge (Behrens et al., 1990; Saal and Van Orman, 2004). Peterson et al. (2014) assumed that the diffusion coefficients for Nb, Zr, and Ti are similar to those of Th and U. Like Peterson et al. (2014), we assumed that Eu is 50% Eu^{2+} , and that the diffusion coefficient for Eu^{2+} is similar to that of Sr.

^cWhile Peterson et al. (2014) used a Galapagos lava to calculate an equilibrium plagioclase composition, we use a Mauna Loa lava (Mauna Loa sample J2-15-13; Wanless et al., 2006). The plagioclase composition in equilibrium with this melt is calculated using the partition coefficients in the table.

^dLike Peterson et al. (2014), the initial melt is a 12% aggregated fractional melt of DMM composition from Workman and Hart (2005), and the isotopic value is the average of the East Pacific Rise Ridge segment averages from Gale et al. (2013).

477 The diffusive exchange model for the high $(\text{Sr}/\text{Ce})_{\text{N}}$ melt inclusions relies on the fact that
 478 the percolating melt is depleted, and this may seem unexpected for a hotspot volcano far from a
 479 MOR. Nonetheless, depleted components have been suggested to exist in the Hawaiian plume
 480 (e.g., Garcia et al., 2010; Harrison et al., 2020). Garcia et al. (2010) hypothesize that an ancient
 481 depleted upper mantle component exists in the Hawaiian plume, that could potentially supply the
 482 depleted percolating melt that interacts with the Mauna Loa gabbro in our model. Additionally,
 483 Mukhopadhyay et al. (2003) state that they “favor an asthenospheric origin for the DM
 484 component” in Hawai’i, and that “the DM component is most apparent in lavas from the Kauai
 485 shield and is present in varying proportion in other Hawaiian shield volcanoes,” including Mauna
 486 Loa (which has ~20% of the DM component in Figure 14 of Mukhopadhyay et al., 2003). As

487 such, evidence exists that supports the existence of a depleted component in the Hawaiian plume
 488 that sources shield stage lavas, consistent with our model. While the precise origin of the
 489 depleted component is unknown, we use the composition of the Workman and Hart (2005)
 490 depleted mantle component to approximate its trace element composition.

491 The results of the melt-plagioclase diffusive exchange model are compared with the
 492 Hawaiian melt inclusion data in Figures 4 and 6, and the model encompasses both the $^{87}\text{Sr}/^{86}\text{Sr}$
 493 composition and the unusual trace element composition—high $(\text{Sr}/\text{Ce})_{\text{N}}$ and low $(\text{La}/\text{Sm})_{\text{N}}$ —of
 494 the Mauna Loa ghost plagioclase inclusion examined here. While diffusive exchange with a
 495 Mauna Loa cumulate gabbro is consistent with the high $(\text{Sr}/\text{Ce})_{\text{N}}$ inclusion data presented here,
 496 the Mauna Loa-like $^{87}\text{Sr}/^{86}\text{Sr}$ in the high $(\text{Sr}/\text{Ce})_{\text{N}}$ inclusion is inconsistent with diffusive
 497 exchange between upwelling melts and MOR-basement gabbro. Diffusive exchange between
 498 melts and MOR-basement gabbro in the Pacific lithosphere would predict low, MORB-like
 499 $^{87}\text{Sr}/^{86}\text{Sr}$ in the melt inclusion. This is because the model predicts that the percolating melt will
 500 rapidly (>5 years; Figure 6) become dominated by the $^{87}\text{Sr}/^{86}\text{Sr}$ of the gabbro, and the average
 501 xenoliths from Hualalai sampling MOR-basement gabbros indicate that the Cretaceous oceanic
 502 crustal gabbros beneath Hawai'i have $^{87}\text{Sr}/^{86}\text{Sr}$ (0.702733 ± 0.000392 (2SD); Gao et al., 2016)
 503 that is indistinguishable from East Pacific Rise MORB (0.70257 ± 0.00024 ; Gale et al., 2013)
 504 due to relatively little modification by seawater. Furthermore, the low Cl/K (<0.01) in the highest
 505 $(\text{Sr}/\text{Ce})_{\text{N}}$ inclusion rules out interaction with seawater-altered MOR gabbro with higher
 506 (secondary) $^{87}\text{Sr}/^{86}\text{Sr}$, because such a model would predict a high Cl/K ratio in the melt
 507 inclusion. Incidentally, Peterson et al. (2014) exclude diffusive melt exchange with MORB-
 508 related gabbros in the Galapagos because this would generate a *negative* Sr anomaly, due to
 509 lower Sr concentrations in oceanic gabbros than melts from oceanic hotspot volcanoes, a result
 510 that is directly applicable to the Hawaiian case examined here. Thus, we can rule out Cretaceous
 511 oceanic crustal gabbro as the origin of the ghost plagioclase signature.

512 An important remaining question is to explore whether the $^{87}\text{Sr}/^{86}\text{Sr}$ we measured in the
 513 Mauna Loa inclusion with the ghost plagioclase signature is consistent with the recycled gabbro
 514 model proposed by Sobolev et al. (2000). We explore this question below.

515 **4.4 Using Sr isotopes to test models for the origin of the ghost plagioclase signature in** 516 **Mauna Loa inclusions.**

517 The primary result of this study is that the Mauna Loa melt inclusion with high $(\text{Sr}/\text{Ce})_{\text{N}}$
 518 is indistinguishable in $^{87}\text{Sr}/^{86}\text{Sr}$ from other melt inclusions from the same lava (sample ML-2012-
 519 27; Figure 6). This melt inclusion also has $^{87}\text{Sr}/^{86}\text{Sr}$ that falls within the range of $^{87}\text{Sr}/^{86}\text{Sr}$
 520 identified in Mauna Loa lavas. We explore the implications of this observation below.

521 While a recycled gabbro signature may be present in the mantle for most Loa-trend
 522 volcanoes, including Mauna Loa (Frey et al., 2016), recycled gabbro is unlikely to have
 523 contributed the high $(\text{Sr}/\text{Ce})_{\text{N}}$ signature to the high $(\text{Sr}/\text{Ce})_{\text{N}}$ Mauna Loa inclusion examined here.
 524 If high $(\text{Sr}/\text{Ce})_{\text{N}}$ is a measure of magnitude of the contribution of the recycled gabbro component,
 525 as proposed by Sobolev et al. (2000), this raises the question as to why the highest $(\text{Sr}/\text{Ce})_{\text{N}}$ melt
 526 inclusion has the same $^{87}\text{Sr}/^{86}\text{Sr}$ as the Mauna Loa melt inclusions and lavas with normal
 527 $(\text{Sr}/\text{Ce})_{\text{N}}$. In their model, the recycled gabbro contributes approximately 73 to 79% of the total Sr
 528 budget in ghost plagioclase melts, which is much larger than gabbro contributions suggested for
 529 Hawaiian lavas. Therefore, if an excess contribution from recycled gabbro were responsible for
 530 the high $(\text{Sr}/\text{Ce})_{\text{N}}$ signature in the unusual, high $(\text{Sr}/\text{Ce})_{\text{N}}$ Mauna Loa melt inclusion examined
 531 here, then the high $(\text{Sr}/\text{Ce})_{\text{N}}$ melt inclusions should have $^{87}\text{Sr}/^{86}\text{Sr}$ that is shifted closer to the

532 $^{87}\text{Sr}/^{86}\text{Sr}$ of the recycled gabbro compositions than the Mauna Loa melt inclusions with normal
 533 $(\text{Sr}/\text{Ce})_{\text{N}}$. This is not observed: The high $(\text{Sr}/\text{Ce})_{\text{N}}$ melt inclusion and inclusions with normal
 534 $(\text{Sr}/\text{Ce})_{\text{N}}$ have indistinguishable $^{87}\text{Sr}/^{86}\text{Sr}$. If one appeals to coincidence, and assumes that the
 535 recycled gabbro has evolved to have exactly the same $^{87}\text{Sr}/^{86}\text{Sr}$ composition as the other
 536 component(s) sampled by the Mauna Loa inclusions with normal $(\text{Sr}/\text{Ce})_{\text{N}}$, then one can explain
 537 why high $(\text{Sr}/\text{Ce})_{\text{N}}$ and normal $(\text{Sr}/\text{Ce})_{\text{N}}$ inclusions from Mauna Loa have the same $^{87}\text{Sr}/^{86}\text{Sr}$.
 538 However, we do not accept such a coincidence as plausible, for two reasons. First, possible
 539 compositions of the ancient recycled gabbro protolith are highly variable—including, but not
 540 limited to, gabbro from recycled seamounts, large igneous provinces, or oceanic lithosphere
 541 (depleted-MORB, normal-MORB, or enriched-MORB)—and thus will run the gamut of Sr-
 542 isotopic compositions, making it unlikely that ancient recycled gabbro would coincidentally evolve
 543 to have $^{87}\text{Sr}/^{86}\text{Sr}$ like Mauna Loa lavas that lack the ghost plagioclase inclusions. Second,
 544 variable dehydration and melting processes operating on heterogeneous protoliths at different
 545 times in distinct subduction zones, followed by varying periods of storage in the mantle and
 546 admixture with diverse reservoirs, are unlikely to generate different components—a high
 547 $(\text{Sr}/\text{Ce})_{\text{N}}$ recycled gabbro component and low $(\text{Sr}/\text{Ce})_{\text{N}}$ components—in the plume with
 548 indistinguishable $^{87}\text{Sr}/^{86}\text{Sr}$. In short, an ancient recycled gabbro component is unlikely to be
 549 responsible for the high $(\text{Sr}/\text{Ce})_{\text{N}}$ “ghost plagioclase” melt inclusions.

550 A more straightforward explanation for the identical $^{87}\text{Sr}/^{86}\text{Sr}$ in the high $(\text{Sr}/\text{Ce})_{\text{N}}$ melt
 551 inclusions and “normal” $(\text{Sr}/\text{Ce})_{\text{N}}$ inclusions in Mauna Loa is that the former inherited the high
 552 $(\text{Sr}/\text{Ce})_{\text{N}}$ signature by interacting with Mauna Loa gabbros. Gabbros related to construction of
 553 the hotspot volcano will have $^{87}\text{Sr}/^{86}\text{Sr}$ ratios that are similar to Mauna Loa lavas, normal-type
 554 inclusions, and the ghost plagioclase inclusion in this study. The diffusive exchange model
 555 generates the high $(\text{Sr}/\text{Ce})_{\text{N}}$ in ghost plagioclase melt inclusions—indicative of plagioclase-melt
 556 interaction—and is also consistent with the relationships between $(\text{Sr}/\text{Ce})_{\text{N}}$ and $^{87}\text{Sr}/^{86}\text{Sr}$ (Figures
 557 4 and 6). This result, which employs Sr isotopic constraints on the origin of ghost plagioclase
 558 melt inclusions, mirrors the findings of Peterson et al. (2014), who also showed that the Pb
 559 isotopic compositions in Galapagos ghost plagioclase melt inclusions are inconsistent with an
 560 ancient recycled oceanic gabbro origin.

561 **5. Conclusion**

562 This study uses Sr isotopic measurements in individual melt inclusions to evaluate the
 563 origin of the ghost plagioclase signature—elevated $(\text{Sr}/\text{Ce})_{\text{N}}$, but similar Al_2O_3 , as melt
 564 inclusions with $(\text{Sr}/\text{Ce})_{\text{N}} < 2$ —in Mauna Loa melt inclusions. The $^{87}\text{Sr}/^{86}\text{Sr}$ of the highest $(\text{Sr}/\text{Ce})_{\text{N}}$
 565 melt inclusion ($(\text{Sr}/\text{Ce})_{\text{N}} = 7.2$) matches the $^{87}\text{Sr}/^{86}\text{Sr}$ in lower $(\text{Sr}/\text{Ce})_{\text{N}}$ melt inclusions ($(\text{Sr}/\text{Ce})_{\text{N}}$
 566 < 2) from the same lava, and is also indistinguishable from $^{87}\text{Sr}/^{86}\text{Sr}$ in Mauna Loa lavas.
 567 Because the highest $(\text{Sr}/\text{Ce})_{\text{N}}$ melt inclusion is isotopically indistinguishable from Mauna Loa
 568 melts with small Sr anomalies, the source of the high $(\text{Sr}/\text{Ce})_{\text{N}}$ melt inclusions should have the
 569 same $^{87}\text{Sr}/^{86}\text{Sr}$ as the component that generates other Mauna Loa lavas with smaller $(\text{Sr}/\text{Ce})_{\text{N}}$
 570 ratios. According to Sobolev et al. (2000), the $^{87}\text{Sr}/^{86}\text{Sr}$ of the recycled gabbro will dominate the
 571 $^{87}\text{Sr}/^{86}\text{Sr}$ signature in ghost plagioclase melt inclusions because the recycled gabbro contributes
 572 to the majority of the total Sr budget in ghost plagioclase melts. While we cannot rule out
 573 recycled gabbro as the source of the ghost plagioclase signature, it would be a great coincidence
 574 that any recycled gabbro component in the Hawaiian mantle plume melting beneath Mauna Loa
 575 would have the same $^{87}\text{Sr}/^{86}\text{Sr}$ as the source of other Mauna Loa lavas that lack a recycled
 576 gabbro signature. Therefore, the observation that the $^{87}\text{Sr}/^{86}\text{Sr}$ of the highest $(\text{Sr}/\text{Ce})_{\text{N}}$ inclusion

577 matches Mauna Loa lavas supports a petrogenetic origin for the ghost plagioclase melt inclusions
 578 that relates to the Mauna Loa magma plumbing system. We find that the origin of the ghost
 579 plagioclase signature within melt inclusions can be explained by diffusive interaction between
 580 rising melt and plagioclase-rich lithologies in the deep magma cumulates of Hawaiian volcanoes.
 581 Thus, the ghost plagioclase signature may not be a signature directly derived from the mantle
 582 source, but instead is likely a result of recent crustal processes operating in the deep regions of
 583 Hawaiian volcanoes.

584 **Acknowledgments and Data**

585 We thank Al Hofmann, Jonathan Snow, Peter Michael, and John Maclennan for reviews;
 586 John Maclennan requested a robust comparison of the TIMS and single-collector ICP-MS
 587 $^{87}\text{Sr}/^{86}\text{Sr}$ datasets on the Puu Wahi melt inclusions. Shichun Huang is acknowledged for
 588 providing thoughtful discussion. OEA acknowledges support from UCSB's Earth Research
 589 Institute for support through the Graduate Student Fellowship. MGJ acknowledges NSF grants
 590 OCE-1736984, EAR-1624840, and EAR-1429648. Gareth Seward's skillful assistance with
 591 UCSB's electron microprobe is gratefully acknowledged. JPM also thanks Mike Garcia and
 592 Aaron Pietruszka for supplying samples. EFR-K thanks J-L. Devidal for his time, advice and
 593 help during the LA-ICPMS analysis and acknowledges the support of the French Government
 594 Laboratory of Excellence initiative ANR-10-LABX-0006. This is Laboratory of Excellence
 595 ClerVolc contribution number xxx. This publication is LANL LA-UR-21-20540. All data
 596 published in this manuscript are available in the EarthChem data repository
 597 (<https://doi.org/10.1594/IEDA/111193> and <https://doi.org/10.26022/IEDA/111591>).

598 **References**

- 599 Bédard, J. H. (2006). Trace element partitioning in plagioclase feldspar. *Geochimica et*
 600 *Cosmochimica Acta*, 70(14), 3717–3742. <https://doi.org/10.1016/j.gca.2006.05.003>
- 601 Behrens, H., Johannes, W., & Schmalzried, H. (1990). On the mechanisms of cation diffusion
 602 processes in ternary feldspars. *Physics and Chemistry of Minerals*, 17(1), 62–78.
 603 <https://doi.org/10.1007/BF00209227>
- 604 Bennett, V. C., Esat, T. M., & Norman, M. D. (1996). Two mantle-plume components in
 605 Hawaiian picrites inferred from correlated Os–Pb isotopes. *Nature*, 381, 221–224.
 606 <https://doi.org/10.1038/381221a0>
- 607 Chauvel, C., & Hémond, C. (2000). Melting of a complete section of recycled oceanic crust:
 608 trace element and Pb isotopic evidence from Iceland. *Geochemistry, Geophysics, Geosystems*,
 609 1(2). <https://doi.org/10.1029/1999GC000002>
- 610 Cherniak, D. J. (1995). Diffusion of lead in plagioclase and K-feldspar: an investigation using
 611 Rutherford backscattering and resonant nuclear reaction analysis. *Contributions to Mineralogy*
 612 *and Petrology*, 120(3–4), 358–371. <https://doi.org/10.1007/BF00306513>

- 613 Cherniak, D. J. (2002). Ba diffusion in feldspar. *Geochimica et Cosmochimica Acta*, 66(9),
614 1641–1650. [https://doi.org/10.1016/S0016-7037\(01\)00866-3](https://doi.org/10.1016/S0016-7037(01)00866-3)
- 615 Cherniak, D. J. (2003). REE diffusion in feldspar. *Chemical Geology*, 193(1–2), 25–41.
616 [https://doi.org/10.1016/S0009-2541\(02\)00246-2](https://doi.org/10.1016/S0009-2541(02)00246-2)
- 617 Cherniak, D. J., & Watson, E. B. (1994). A study of strontium diffusion in plagioclase using
618 Rutherford backscattering spectroscopy. *Geochimica et Cosmochimica Acta*, 58(23), 5179–5190.
619 [https://doi.org/10.1016/0016-7037\(94\)90303-4](https://doi.org/10.1016/0016-7037(94)90303-4)
- 620 Colman, A., Sinton, J. M., & Wanless, V. D. (2015). Constraints from melt inclusions on depths
621 of magma residence at intermediate magma supply along the Galápagos Spreading Center. *Earth
622 and Planetary Science Letters*, 412, 122–131. <https://doi.org/10.1016/j.epsl.2014.12.007>
- 623 Cooper, K. M., Reid, M. R., Murrell, M. T., & Clague, D. A. (2001). Crystal and magma
624 residence at Kilauea Volcano, Hawaii: 230Th–226Ra dating of the 1955 east rift eruption. *Earth
625 and Planetary Science Letters*, 184(3–4), 703–718. [https://doi.org/10.1016/S0012-
626 821X\(00\)00341-1](https://doi.org/10.1016/S0012-821X(00)00341-1)
- 627 Danyushevsky, L. V., Della-Pasqua, F. N., & Sokolov, S. (2000). Re-equilibration of melt
628 inclusions trapped by magnesian olivine phenocrysts from subduction-related magmas:
629 petrological implications. *Contributions to Mineralogy and Petrology*, 138(1), 68–83.
630 <https://doi.org/10.1007/PL00007664>
- 631 Danyushevsky, L. V., Leslie, R. A., Crawford, A. J., & Durance, P. (2004). Melt inclusions in
632 primitive olivine phenocrysts: the role of localized reaction processes in the origin of anomalous
633 compositions. *Journal of Petrology*, 45(12), 2531–2553.
634 <https://doi.org/10.1093/petrology/egh080>
- 635 Danyushevsky, L. V., Perfit, M. R., Eggins, S. M., & Falloon, T. J. (2003). Crustal origin for
636 coupled 'ultra-depleted' and 'plagioclase' signatures in MORB olivine-hosted melt inclusions:
637 evidence from the Siqueiros Transform Fault, East Pacific Rise. *Contributions to Mineralogy
638 and Petrology*, 144(5), 619–637. <https://doi.org/10.1007/s00410-002-0420-3>
- 639 Debret, B., Koga, K. T., Nicollet, C., Andreani, M., & Schwartz, S. (2014). F, Cl and S input via
640 serpentinite in subduction zones: Implications for the nature of the fluid released at depth. *Terra
641 Nova*, 26(2), 96–101. <https://doi.org/10.1111/ter.12074>.
- 642 Ford, C. E., Russell, D. G., Craven, J. A., & Fisk, M. R. (1983). Olivine-liquid equilibria:
643 temperature, pressure and composition dependence of the crystal/liquid cation partition
644 coefficients for Mg, Fe²⁺, Ca and Mn. *Journal of Petrology*, 24(3), 256–266.
645 <https://doi.org/10.1093/petrology/24.3.256>

- 646 Frey, F. A., Huang, S., Xu, G., & Jochum, K. P. (2016). The geochemical components that
647 distinguish Loa-and Kea-trend Hawaiian shield lavas. *Geochimica et Cosmochimica Acta*, 185,
648 160–181. <https://doi.org/10.1016/j.gca.2016.04.010>
- 649 Gaetani, G. A., & Watson, E. B. (2000). Open system behavior of olivine-hosted melt inclusions.
650 *Earth and Planetary Science Letters*, 183(1–2), 27–41. [https://doi.org/10.1016/S0012-](https://doi.org/10.1016/S0012-821X(00)00260-0)
651 821X(00)00260-0
- 652 Gaffney, A. M. (2002). Environments of crystallization and compositional diversity of Mauna
653 Loa xenoliths. *Journal of Petrology*, 43(6), 963–981. <https://doi.org/10.1093/petrology/43.6.963>
- 654 Gagnon, J. E., Fryer, B. J., Samson, I. M., & Williams-Jones, A. E. (2008). Quantitative analysis
655 of silicate certified reference materials by LA-ICPMS with and without an internal standard.
656 *Journal of Analytical Atomic Spectrometry*, 23(11), 1529–1537.
657 <https://doi.org/10.1039/B801807N>
- 658 Gale, A., Dalton, C. A., Langmuir, C. H., Su, Y., & Schilling, J. (2013). The mean composition
659 of ocean ridge basalts. *Geochemistry, Geophysics, Geosystems*, 14(3), 489–518,
660 <https://doi.org/10.1029/2012GC004334>
- 661 Gansecki, C., Lee, R. L., Shea, T., Lundblad, S. P., Hon, K., & Parcheta, C. (2019). The tangled
662 tale of Kīlauea’s 2018 eruption as told by geochemical monitoring. *Science*, 366(6470).
663 <https://doi.org/10.1126/science.aaz0147>
- 664 Gao, R., Lassiter, J. C., Barnes, J. D., Clague, D. A., & Bohrsen, W. A. (2016). Geochemical
665 investigation of Gabbroic Xenoliths from Hualalai Volcano: Implications for lower oceanic crust
666 accretion and Hualalai Volcano magma storage system. *Earth and Planetary Science Letters*,
667 442, 162–172. <https://doi.org/10.1016/j.epsl.2016.02.043>
- 668 Garcia, M. O., Foss, D. J., West, H. B., & Mahoney, J. J. (1995). Geochemical and isotopic
669 evolution of Loihi Volcano, Hawaii. *Journal of Petrology*, 36(6), 1647–1674.
670 <https://doi.org/10.1093/oxfordjournals.petrology.a037269>
- 671 Garcia, M. O., Jorgenson, B. A., Mahoney, J. J., Ito, E., & Irving, A. J. (1993). An evaluation of
672 temporal geochemical evolution of Loihi summit lavas: results from Alvin submersible dives.
673 *Journal of Geophysical Research: Solid Earth*, 98 (B1), 537–550.
674 <https://doi.org/10.1029/92JB01707>
- 675 Garcia, M. O., Swinnard, L., Weis, D., Greene, A. R., Tagami, T., Sano, H., & Gandy, C. E.
676 (2010). Petrology, geochemistry and geochronology of Kaua’i lavas over 4.5 Myr: Implications
677 for the origin of rejuvenated volcanism and the evolution of the Hawaiian plume. *Journal of*
678 *Petrology*, 51(7), 1507–1540. <https://doi.org/10.1093/petrology/egq027>

- 679 Garcia, M. O., Rubin, K. H., Norman, M. D., Rhodes, J. M., Graham, D. W., Muenow, D. W., &
 680 Spencer, K. (1998). Petrology and geochronology of basalt breccia from the 1996 earthquake
 681 swarm of Loihi seamount, Hawaii: magmatic history of its 1996 eruption. *Bulletin of*
 682 *Volcanology*, 59(8), 577–592. <https://doi.org/10.1007/s004450050211>
- 683 Giletti, B. J., & Casserly, J. E. D. (1994). Strontium diffusion kinetics in plagioclase feldspars.
 684 *Geochimica et Cosmochimica Acta*, 58(18), 3785–3793. [https://doi.org/10.1016/0016-](https://doi.org/10.1016/0016-7037(94)90363-8)
 685 [7037\(94\)90363-8](https://doi.org/10.1016/0016-7037(94)90363-8)
- 686 Giletti, B. J., & Shanahan, T. M. (1997). Alkali diffusion in plagioclase feldspar. *Chemical*
 687 *Geology*, 139(1–4), 3–20. [https://doi.org/10.1016/S0009-2541\(97\)00026-0](https://doi.org/10.1016/S0009-2541(97)00026-0)
- 688 Gurenko, A. A., & Chaussidon, M. (1995). Enriched and depleted primitive melts included in
 689 olivine from Icelandic tholeiites: origin by continuous melting of a single mantle column.
 690 *Geochimica et Cosmochimica Acta*, 59(14), 2905–2917. [https://doi.org/10.1016/0016-](https://doi.org/10.1016/0016-7037(95)00184-0)
 691 [7037\(95\)00184-0](https://doi.org/10.1016/0016-7037(95)00184-0)
- 692 Harlou, R., Pearson, D. G., Nowell, G. M., Ottley, C. J., & Davidson, J. P. (2009). Combined Sr
 693 isotope and trace element analysis of melt inclusions at sub-ng levels using micro-milling, TIMS
 694 and ICPMS. *Chemical Geology*, 260(3–4), 254–268.
 695 <https://doi.org/10.1016/j.chemgeo.2008.12.020>
- 696 Harrison, L. N., Weis, D., & Garcia, M. O. (2020). The multiple depleted mantle components in
 697 the Hawaiian-Emperor chain. *Chemical Geology*, 532, 119324.
 698 <https://doi.org/10.1016/j.chemgeo.2019.119324>
- 699 Hauri, E. H. (1996). Major-element variability in the Hawaiian mantle plume. *Nature*,
 700 382(6590), 415–419. <https://doi.org/10.1038/382415a0>
- 701 Hauri, E. H., Lassiter, J. C., & DePaolo, D. J. (1996). Osmium isotope systematics of drilled
 702 lavas from Mauna Loa, Hawaii. *Journal of Geophysical Research: Solid Earth*, 101(B5), 11793–
 703 11806. <https://doi.org/10.1029/95JB03346>
- 704 Hofmann, A. W., & Jochum, K. P. (1996). Source characteristics derived from very incompatible
 705 trace elements in Mauna Loa and Mauna Kea basalts, Hawaii Scientific Drilling Project. *Journal*
 706 *of Geophysical Research: Solid Earth*, 101(B5), 11831–11839.
 707 <https://doi.org/10.1029/95JB03701>
- 708 Huang, S., & Humayun, M. (2016). Petrogenesis of high-CaO lavas from Mauna Kea, Hawaii:
 709 Constraints from trace element abundances. *Geochimica et Cosmochimica Acta*, 185, 198–215.
 710 <https://doi.org/10.1016/j.gca.2016.03.039>

- 711 Jackson, M. G., & Hart, S. R. (2006). Strontium isotopes in melt inclusions from Samoan
712 basalts: Implications for heterogeneity in the Samoan plume. *Earth and Planetary Science*
713 *Letters*, 245(1–2), 260–277. <https://doi.org/10.1016/j.epsl.2006.02.040>
- 714 Jambon, A., Déruelle, B., Dreibus, G., & Pineau, F. (1995). Chlorine and bromine abundance in
715 MORB: the contrasting behaviour of the Mid-Atlantic Ridge and East Pacific Rise and
716 implications for chlorine geodynamic cycle. *Chemical Geology*, 126(2), 101–117.
717 [https://doi.org/10.1016/0009-2541\(95\)00112-4](https://doi.org/10.1016/0009-2541(95)00112-4)
- 718 Jochum, K. P., Stoll, B., Herwig, K., Willbold, M., Hofmann, A. W., Amini, M., et al. (2006).
719 MPI-DING reference glasses for in situ microanalysis: New reference values for element
720 concentrations and isotope ratios. *Geochemistry, Geophysics, Geosystems*, 7(2).
721 <https://doi.org/10.1029/2005GC001060>
- 722 Jochum, K. P., Stoll, B., Weis, U., Kuzmin, D. V., & Sobolev, A. V. (2009). In situ Sr isotopic
723 analysis of low Sr silicates using LA-ICP-MS. *Journal of Analytical Atomic Spectrometry*, 24(9),
724 1237–1243. <https://doi.org/10.1039/B905045K>
- 725 John, T., Scambelluri, M., Frische, M., Barnes, J. D., & Bach, W. (2011). Dehydration of
726 subducting serpentinite: Implications for halogen mobility in subduction zones and the deep
727 halogen cycle. *Earth and Planetary Science Letters*, 308(1–2), 65–76,
728 <https://doi.org/10.1016/j.epsl.2011.05.038>
- 729 Kendrick, M. A., Arculus, R., Burnard, P., & Honda, M. (2013a). Quantifying brine assimilation
730 by submarine magmas: Examples from the Galápagos Spreading Centre and Lau Basin.
731 *Geochimica et Cosmochimica Acta*, 123, 150–165. <https://doi.org/10.1016/j.gca.2013.09.012>
- 732 Kendrick, M. A., Hémond, C., Kamenetsky, V. S., Danyushevsky, L., Devey, C. W., Rodemann,
733 T., Jackson, M. G., & Perfit, M. R. (2017). Seawater cycled throughout Earth's mantle in
734 partially serpentinitized lithosphere. *Nature Geoscience*, 10(3), 222–228.
735 <https://doi.org/10.1038/ngeo2902>
- 736 Kendrick, M. A., Honda, M., Pettke, T., Scambelluri, M., Phillips, D., & Giuliani, A. (2013b).
737 Subduction zone fluxes of halogens and noble gases in seafloor and forearc serpentinites, *Earth*
738 *and Planetary Science Letters*, 365, 86–96, <https://doi.org/10.1016/j.epsl.2013.01.006>.
- 739 Kendrick, M. A., Jackson, M. G., Hauri, E. H., & Phillips, D. (2015). The halogen (F, Cl, Br, I)
740 and H₂O systematics of Samoan lavas: Assimilated-seawater, EM2 and high-³He/⁴He
741 components. *Earth and Planetary Science Letters*, 410, 197–209.
742 <https://doi.org/10.1016/j.epsl.2014.11.026>
- 743 Kent, A. J. R. (2008). Melt inclusions in basaltic and related volcanic rocks. *Reviews in*
744 *Mineralogy and Geochemistry*, 69(1), 273–331. <https://doi.org/10.2138/rmg.2008.69.8>

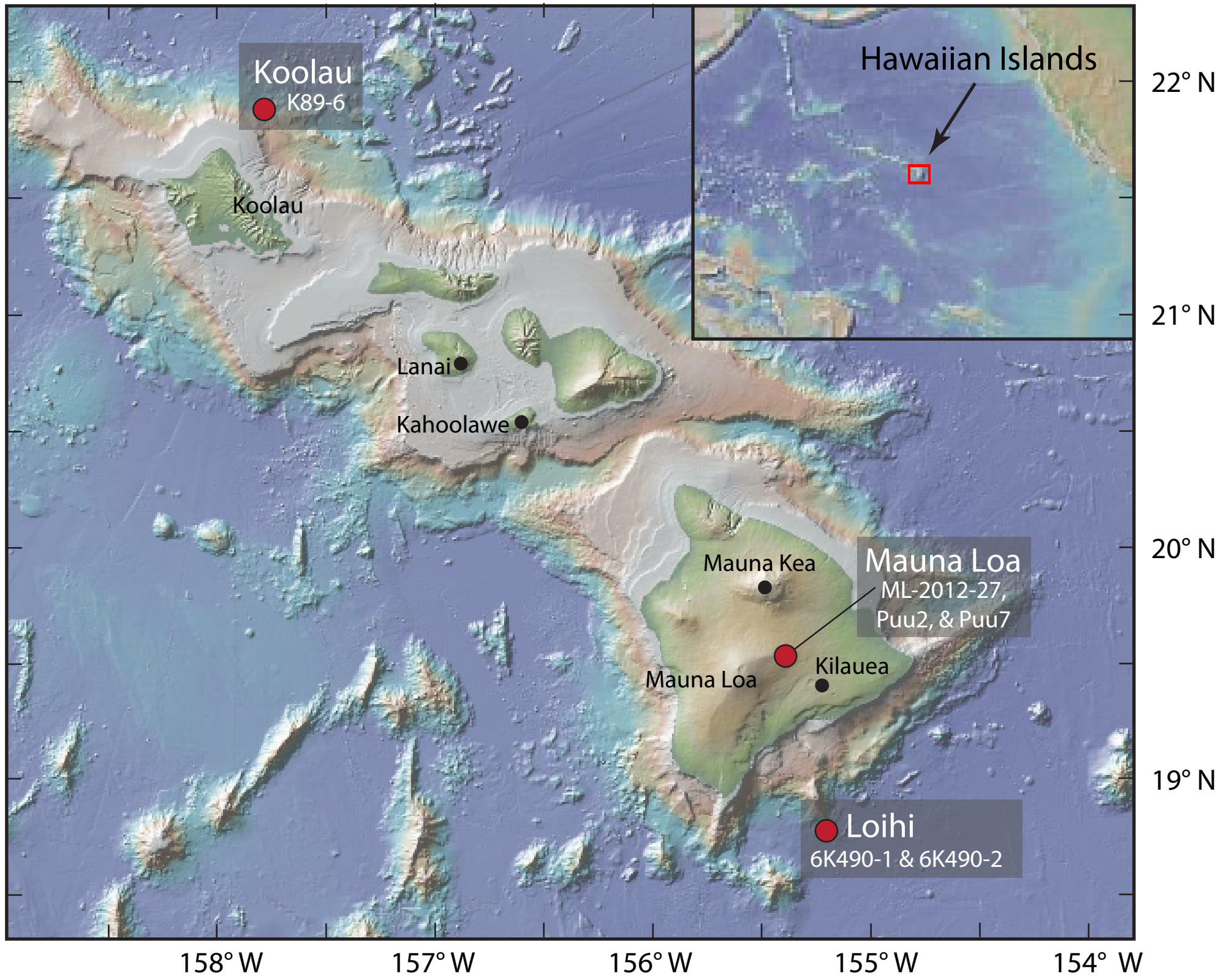
- 745 Kent, A. J. R., Clague, D. A., Honda, M., Stolper, E. M., Hutcheon, I. D., & Norman, M. D.
746 (1999a). Widespread assimilation of a seawater-derived component at Loihi Seamount, Hawaii.
747 *Geochimica et Cosmochimica Acta*, 63(18), 2749–2761. [https://doi.org/10.1016/S0016-](https://doi.org/10.1016/S0016-7037(99)00215-X)
748 7037(99)00215-X
- 749 Kent, A. J. R., Norman, M. D., Hutcheon, I. D., & Stolper, E. M. (1999b). Assimilation of
750 seawater-derived components in an oceanic volcano: evidence from matrix glasses and glass
751 inclusions from Loihi seamount, Hawaii. *Chemical Geology*, 156(1–4), 299–319.
752 [https://doi.org/10.1016/S0009-2541\(98\)00188-0](https://doi.org/10.1016/S0009-2541(98)00188-0)
- 753 Kent, A. J. R., Peate, D. W., Newman, S., Stolper, E. M., & Pearce, J. A. (2002). Chlorine in
754 submarine glasses from the Lau Basin: seawater contamination and constraints on the
755 composition of slab-derived fluids. *Earth and Planetary Science Letters*, 202(2), 361–377.
756 [https://doi.org/10.1016/S0012-821X\(02\)00786-0](https://doi.org/10.1016/S0012-821X(02)00786-0)
- 757 Kogiso, T., & Hirschmann, M. M. (2001). Experimental study of clinopyroxenite partial melting
758 and the origin of ultra-calcic melt inclusions. *Contributions to Mineralogy and Petrology*,
759 142(3), 347–360. <https://doi.org/10.1007/s004100100295>
- 760 Koleszar, A. M., Saal, A. E., Hauri, E. H., Nagle, A. N., Liang, Y., & Kurz, M. D. (2009). The
761 volatile contents of the Galapagos plume; evidence for H₂O and F open system behavior in melt
762 inclusions. *Earth and Planetary Science Letters*, 287(3–4), 442–452.
763 <https://doi.org/10.1016/j.epsl.2009.08.029>
- 764 Koornneef, J. M., Nikogosian, I., van Bergen, M. J., Smeets, R., Bouman, C., and Davies, G. R.
765 (2015). TIMS analysis of Sr and Nd isotopes in melt inclusions from Italian potassium-rich lavas
766 using prototype 10¹³ Ω amplifiers. *Chemical Geology*, 397, 14–23,
767 <https://doi.org/10.1016/j.chemgeo.2015.01.005>
- 768 Kurz, M. D., Kenna, T. C., Kammer, D. P., Rhodes, J. M., & Garcia, M. O. (1995). Isotopic
769 evolution of Mauna Loa Volcano: A view from the submarine southwest rift zone. *Geophysical*
770 *Monograph-American Geophysical Union*, 92, 289–306.
- 771 Lassiter, J. C., Hauri, E. H., Nikogosian, I. K., & Barseczus, H. G. (2002). Chlorine–potassium
772 variations in melt inclusions from Raivavae and Rapa, Austral Islands: constraints on chlorine
773 recycling in the mantle and evidence for brine-induced melting of oceanic crust. *Earth and*
774 *Planetary Science Letters*, 202(3–4), 525–540. [https://doi.org/10.1016/S0012-821X\(02\)00826-9](https://doi.org/10.1016/S0012-821X(02)00826-9)
- 775 Lockwood, J. P. (1995). Mauna Loa eruptive history: The preliminary radiocarbon record, *in*
776 Rhodes, J.M., and Lockwood, J.P., eds., *Mauna Loa Revealed: Structure, Composition, History,*
777 *and Hazards. American Geophysical Union Geophysical Monograph*, 92, 81–94,
778 <https://doi.org/10.1029/GM092p0081>

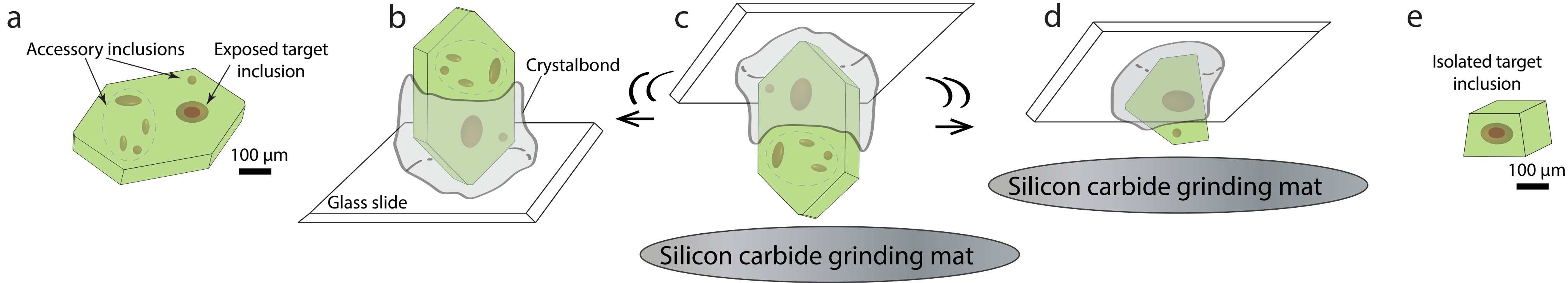
- 779 Maclennan, J. (2008). Lead isotope variability in olivine-hosted melt inclusions from Iceland.
 780 *Geochimica et Cosmochimica Acta*, 72(16), 4159–4176.
 781 <https://doi.org/10.1016/j.gca.2008.05.034>
- 782 Marske, J., & Hauri, E. (2019). Major- and trace-element compositions of 915 melt inclusions
 783 and host olivines from Hawaiian shield volcanoes, Version 1.0. Interdisciplinary Earth Data
 784 Alliance (IEDA). <https://doi.org/10.1594/IEDA/111193>. Accessed 2019-11-06.
- 785 McDonough, W. F., & Sun, S. S. (1995). The composition of the Earth. *Chemical Geology*, 120,
 786 223–253. [https://doi.org/10.1016/0009-2541\(94\)00140-4](https://doi.org/10.1016/0009-2541(94)00140-4)
- 787 Melson, W. G., O'Hearn, T., & Jarosewich, E. (2002). A data brief on the Smithsonian abyssal
 788 volcanic glass data file. *Geochemistry, Geophysics, Geosystems*, 3(4), 1–11.
 789 <https://doi.org/10.1029/2001GC000249>
- 790 Michael, P. J., & Cornell, W. C. (1998). Influence of spreading rate and magma supply on
 791 crystallization and assimilation beneath mid-ocean ridges: Evidence from chlorine and major
 792 element chemistry of mid-ocean ridge basalts. *Journal of Geophysical Research: Solid Earth*,
 793 103(B8), 18325–18356. <https://doi.org/10.1029/98JB00791>
- 794 Michael, P. J., McDonough, W. F., Nielsen, R. L., & Cornell, W. C. (2002). Depleted melt
 795 inclusions in MORB plagioclase: messages from the mantle or mirages from the magma
 796 chamber?. *Chemical Geology*, 183(1–4), 43–61. [https://doi.org/10.1016/S0009-2541\(01\)00371-0](https://doi.org/10.1016/S0009-2541(01)00371-0)
- 797 Mukhopadhyay, S., Lassiter, J. C., Farley, K. A., & Bogue, S. W. (2003). Geochemistry of Kauai
 798 shield-stage lavas: Implications for the chemical evolution of the Hawaiian plume.
 799 *Geochemistry, Geophysics, Geosystems*, 4(1).
- 800 Müller, R. D., Sdrolias, M., Gaina, C., & Roest, W. R. (2008). Age, spreading rates, and
 801 spreading asymmetry of the world's ocean crust. *Geochemistry, Geophysics, Geosystems*, 9(4).
 802 <https://doi.org/10.1029/2007GC001743>
- 803 Peterson, M. E., Saal, A. E., Nakamura, E., Kitagawa, H., Kurz, M. D., & Koleszar, A. M.
 804 (2014). Origin of the ‘ghost plagioclase’ signature in Galapagos melt inclusions: new evidence
 805 from Pb isotopes. *Journal of Petrology*, 55(11), 2193–2216.
 806 <https://doi.org/10.1093/petrology/egu054>
- 807 Pietruszka, A. J., Keyes, M. J., Duncan, J. A., Hauri, E. H., Carlson, R. W., & Garcia, M. O.
 808 (2011). Excesses of seawater-derived ²³⁴U in volcanic glasses from Loihi Seamount due to
 809 crustal contamination. *Earth and Planetary Science Letters*, 304(1–2), 280–289.
 810 <https://doi.org/10.1016/j.epsl.2011.02.018>

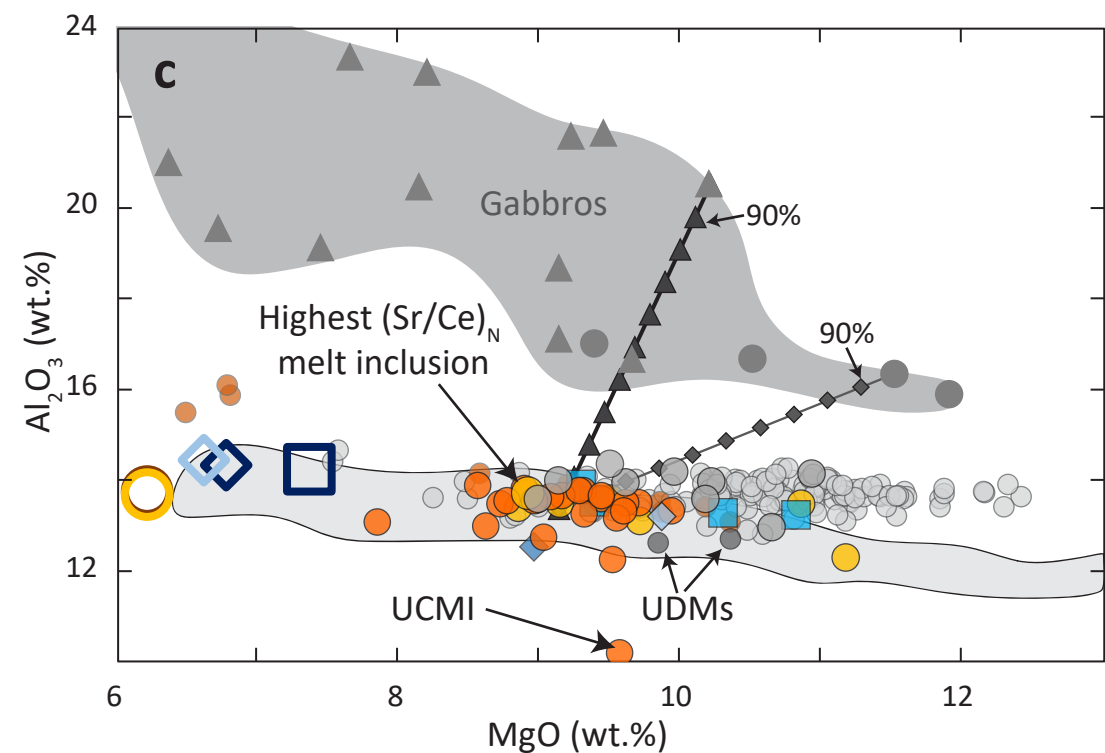
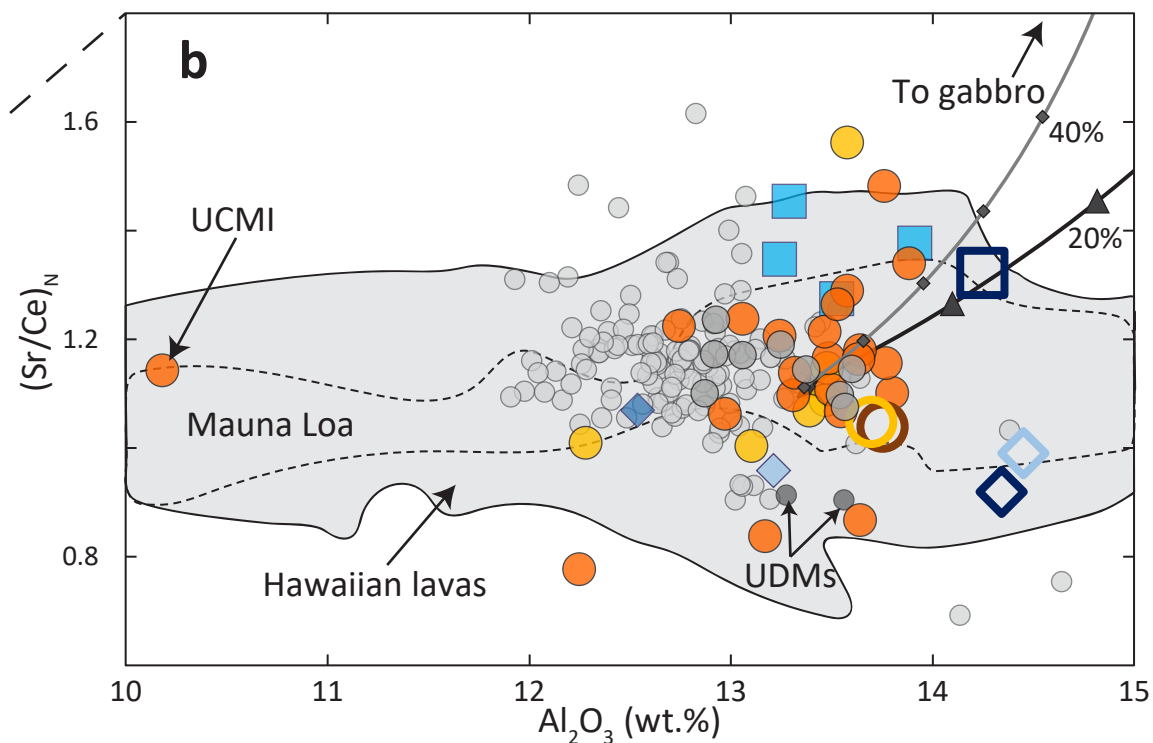
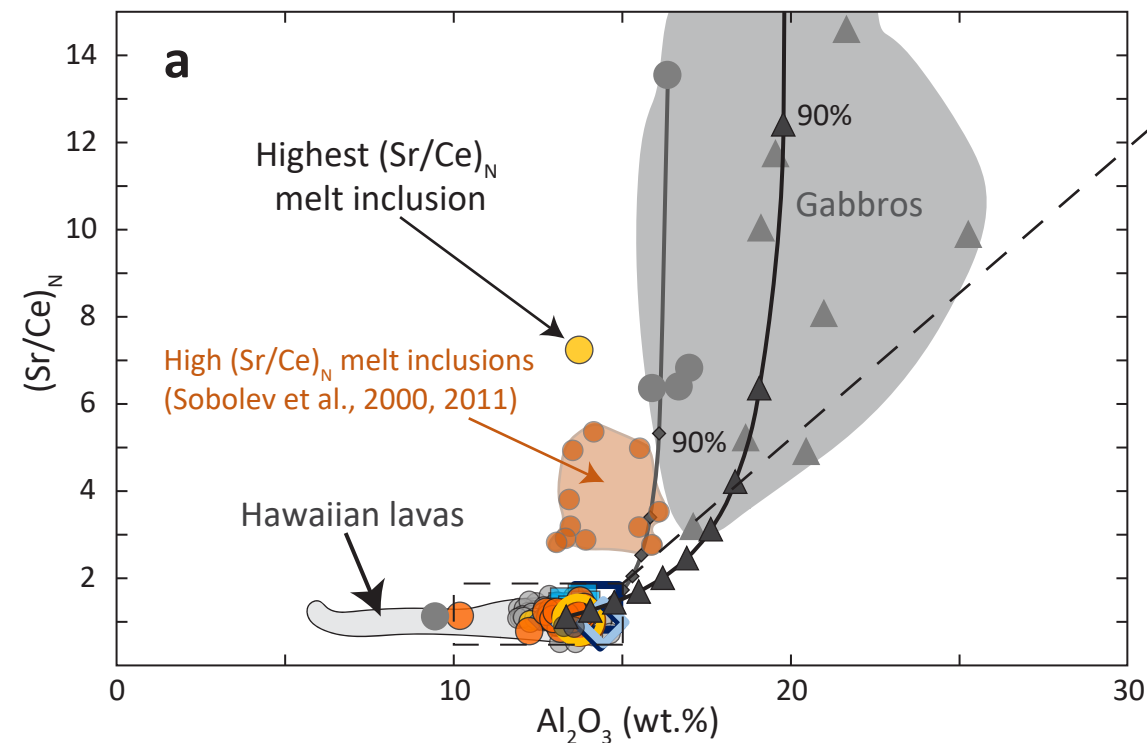
- 811 Price, A. A., Jackson, M. G., Blichert-Toft, J., Blusztajn, J., Conatser, C. S., Konter, J. G.,
 812 Koppers, A. A., & Kurz, M. D. (2016). Geochemical evidence in the northeast Lau Basin for
 813 subduction of the Cook-Austral volcanic chain in the Tonga Trench. *Geochemistry, Geophysics,*
 814 *Geosystems*, 17(5), 1694–1724. <https://doi.org/10.1002/2015GC006237>
- 815 Price, A. A., Jackson, M. G., Blichert-Toft, J., Hall, P. S., Sinton, J. M., Kurz, M. D., &
 816 Blusztajn, J. (2014). Evidence for a broadly distributed Samoan-plume signature in the northern
 817 Lau and North Fiji Basins. *Geochemistry, Geophysics, Geosystems*, 15(4), 986–1008.
 818 <https://doi.org/10.1002/2013GC005061>
- 819 Reinhard, A. A., Jackson, M. G., Harvey, J., Brown, C., & Koornneef, J. M. (2016). Extreme
 820 differences in $^{87}\text{Sr}/^{86}\text{Sr}$ between magmatic olivines and Samoan host lavas: Evidence for highly
 821 heterogeneous $^{87}\text{Sr}/^{86}\text{Sr}$ in the magmatic plumbing system sourcing a single lava. *Chemical*
 822 *Geology*, 438, 120–131. <https://doi.org/10.1016/j.chemgeo.2016.05.017>
- 823 Reinhard, A. A., Jackson, M. G., Koornneef, J. M., Rose-Koga, E. F., Blusztajn, J., Konter, J. G.,
 824 Koga, K. T., Wallace, P. J. & Harvey, J. (2018). Sr and Nd isotopic compositions of individual
 825 olivine-hosted melt inclusions from Hawai'i and Samoa: Implications for the origin of isotopic
 826 heterogeneity in melt inclusions from OIB lavas. *Chemical Geology*, 495, 36–49.
 827 <https://doi.org/10.1016/j.chemgeo.2018.07.034>
- 828 Roden, M. F., Trull, T., Hart, S. R., & Frey, F. A. (1994). New He, Nd, Pb, and Sr isotopic
 829 constraints on the constitution of the Hawaiian plume: Results from Koolau Volcano, Oahu,
 830 Hawaii, USA. *Geochimica et Cosmochimica Acta*, 58(5), 1431–1440.
 831 [https://doi.org/10.1016/0016-7037\(94\)90547-9](https://doi.org/10.1016/0016-7037(94)90547-9)
- 832 Rose-Koga, E. F., Koga, K. T., Schiano, P., Le Voyer, M., Shimizu, N., Whitehouse, M. J., &
 833 Clocchiatti, R. (2012). Mantle source heterogeneity for South Tyrrhenian magmas revealed by
 834 Pb isotopes and halogen contents of olivine-hosted melt inclusions. *Chemical Geology*, 334,
 835 266–279. <https://doi.org/10.1016/j.chemgeo.2012.10.033>
- 836 Rowe, M. C., & Lassiter, J. C. (2009). Chlorine enrichment in central Rio Grande Rift basaltic
 837 melt inclusions: Evidence for subduction modification of the lithospheric mantle. *Geology*,
 838 37(5), 439–442. <https://doi.org/10.1130/G25530A.1>
- 839 Rowe, M. C., Lassiter, J. C., & Goff, K. (2015). Basalt volatile fluctuations during continental
 840 rifting: An example from the Rio Grande Rift, USA. *Geochemistry, Geophysics, Geosystems*,
 841 16(5), 1254–1273. <https://doi.org/10.1002/2014GC005649>
- 842 Ryan, W. B. F., Carbotte, S. M., Coplan, J. O., O'Hara, S., Melkonian, A., Arko, R., Weissel, R.
 843 A., Ferrini, V., Goodwillie, A., Nitsche, F., Bonczkowski, J., & Zemsky, R. (2009). Global

- 844 Multi-Resolution Topography synthesis. *Geochemistry, Geophysics, Geosystems*, 10, Q03014.
845 <https://doi.org/10.1029/2008GC002332>
- 846 Saal, A. E., Hauri, E. H., Langmuir, C. H., & Perfit, M. R. (2002). Vapour undersaturation in
847 primitive mid-ocean-ridge basalt and the volatile content of Earth's upper mantle. *Nature*,
848 419(6906), 451–455. <https://doi.org/10.1038/nature01073>
- 849 Saal, A. E., Kurz, M. D., Hart, S. R., Blusztajn, J. S., Blichert-Toft, J., Liang, Y., & Geist, D. J.
850 (2007). The role of lithospheric gabbros on the composition of Galapagos lavas. *Earth and*
851 *Planetary Science Letters*, 257(3–4), 391–406. <https://doi.org/10.1016/j.epsl.2007.02.040>
- 852 Saal, A. E., & Van Orman, J. A. (2004). The ²²⁶Ra enrichment in oceanic basalts: Evidence for
853 melt-cumulate diffusive interaction processes within the oceanic lithosphere. *Geochemistry,*
854 *Geophysics, Geosystems*, 5(2). <https://doi.org/10.1029/2003GC000620>
- 855 Slater, L., McKenzie, D. A. N., Grönvold, K., & Shimizu, N. (2001). Melt generation and
856 movement beneath Theistareykir, NE Iceland. *Journal of Petrology*, 42(2), 321–354.
857 <https://doi.org/10.1093/petrology/42.2.321>
- 858 Sobolev, A. V., & Danyushevsky, L. V. (1994). Petrology and geochemistry of boninites from
859 the north termination of the Tonga Trench: constraints on the generation conditions of primary
860 high-Ca boninite magmas. *Journal of Petrology*, 35(5), 1183–1211.
861 <https://doi.org/10.1093/petrology/35.5.1183>
- 862 Sobolev, A. V., Hofmann, A. W., Jochum, K. P., Kuzmin, D. V., & Stoll, B. (2011). A young
863 source for the Hawaiian plume. *Nature*, 476, 434–437. <https://doi.org/10.1038/nature10321>
- 864 Sobolev, A. V., Hofmann, A. W., & Nikogosian, I. K. (2000). Recycled oceanic crust observed
865 in ‘ghost plagioclase’ within the source of Mauna Loa lavas. *Nature*, 404, 986–990.
866 <https://doi.org/10.1038/35010098>
- 867 Stone, W. E., & Fleet, M. E. (1991). Nickel-copper sulfides from the 1959 eruption of Kilauea
868 Volcano, Hawaii: Contrasting compositions and phase relations in eruption pumice and Kilauea
869 Iki lava lake. *American Mineralogist*, 76(7–8), 1363–1372.
- 870 Straub, S. M., & Layne, G. D. (2003). The systematics of chlorine, fluorine, and water in Izu arc
871 front volcanic rocks: Implications for volatile recycling in subduction zones. *Geochimica et*
872 *Cosmochimica Acta*, 67(21), 4179–4203. [https://doi.org/10.1016/S0016-7037\(03\)00307-7](https://doi.org/10.1016/S0016-7037(03)00307-7)
- 873 Stroncik, N. A., & Haase, K. M. (2004). Chlorine in oceanic intraplate basalts: Constraints on
874 mantle sources and recycling processes. *Geology*, 32(11), 945–948.
875 <https://doi.org/10.1130/G21027.1>

- 876 Tanaka, R., Nakamura, E., & Takahashi, E. (2002). Geochemical evolution of Koolau volcano,
877 Hawaii. *Geophysical Monograph-American Geophysical Union*, 128, 311–332.
- 878 Thirlwall, M.F. (1991). Long-term reproducibility of multicollector Sr and Nd isotope ratio
879 analysis. *Chemical Geology*, 94, 85–104. [https://doi.org/10.1016/0168-9622\(91\)90002-E](https://doi.org/10.1016/0168-9622(91)90002-E)
- 880 Tucker, J. M., Hauri, E. H., Pietruszka, A. J., Garcia, M. O., Marske, J. P., & Trusdell, F. A.
881 (2019). A high carbon content of the Hawaiian mantle from olivine-hosted melt inclusions.
882 *Geochimica et Cosmochimica Acta*, 254, 156–172. <https://doi.org/10.1016/j.gca.2019.04.001>
- 883 Vinet, N., & Higgins, M. D. (2010). Magma solidification processes beneath Kilauea volcano,
884 Hawaii: A quantitative textural and geochemical study of the 1969–1974 Mauna Ulu Lavas.
885 *Journal of Petrology*, 51(6), 1297–1332. <https://doi.org/10.1093/petrology/egq020>
- 886 Wanless, V. D., Garcia, M. O., Rhodes, J. M., Weis, D., & Norman, M. D. (2006). Shield-stage
887 alkalic volcanism on Mauna Loa volcano, Hawaii. *Journal of Volcanology and Geothermal*
888 *Research*, 151(1–3), 141–155. <https://doi.org/10.1016/j.jvolgeores.2005.07.027>
- 889 Weis, D., Kieffer, B., Maerschalk, C., Barling, J., de Jong, J., Williams, G. A., Hanano, D.,
890 Pretorius, W., Mattielli, N., Scoates, J. S., Goolaerts, A., Friedman, R. M., & Mahoney, J. B.
891 (2006). High-precision isotopic characterization of USGS reference materials by TIMS and MC-
892 ICP-MS. *Geochemistry, Geophysics, Geosystems*, 7(8), Q08006.
893 <https://doi.org/10.1029/2006GC001283>
- 894 Wieser, P. E., Edmonds, M., Maclennan, J., Jenner, F. E., & Kunz, B. E. (2019). Crystal
895 scavenging from mush piles recorded by melt inclusions. *Nature Communications*, 10(1), 1–11.
896 <https://doi.org/10.1038/s41467-019-13518-2>
- 897 Workman, R. K., & Hart, S. R. (2005). Major and trace element composition of the depleted
898 MORB mantle (DMM). *Earth and Planetary Science Letters*, 231(1–2), 53–72.
899 <https://doi.org/10.1016/j.epsl.2004.12.005>
- 900 Yaxley, G. M., & Green, D. H. (1998). Reactions between eclogite and peridotite: mantle
901 refertilisation by subduction of oceanic crust. *Schweizerische mineralogische und*
902 *petrographische Mitteilungen*, 78(2), 243–255.
- 903 Yaxley, G. M., & Sobolev, A. V. (2007). High-pressure partial melting of gabbro and its role in
904 the Hawaiian magma source. *Contributions to Mineralogy and Petrology*, 154(4), 371–383.
905 <https://doi.org/10.1007/s00410-007-0198-4>
- 906 Zimmer, M., Kröner, A., Jochum, K. P., Reischmann, T., & Todt, W. (1995). The Gabal Gerf
907 complex: a Precambrian N-MORB ophiolite in the Nubian shield, NE Africa. *Chemical Geology*,
908 123(1–4), 29–51. [https://doi.org/10.1016/0009-2541\(95\)00018-H](https://doi.org/10.1016/0009-2541(95)00018-H)



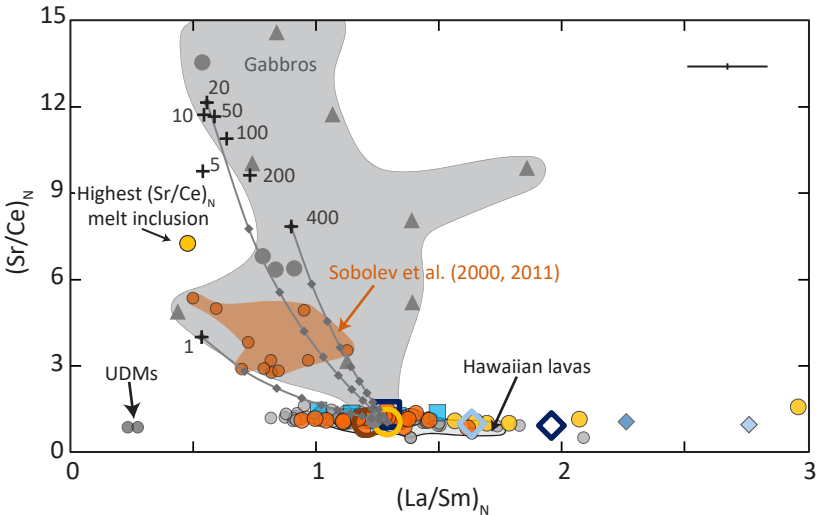




Sample	Melt inclusions	Glass	Volcano
ML-2012-27			Mauna Loa
Puu2 & Puu7			Mauna Loa
6K490-1			Loihi
6K490-2			Loihi
K89-6			Koolau

Previously published data

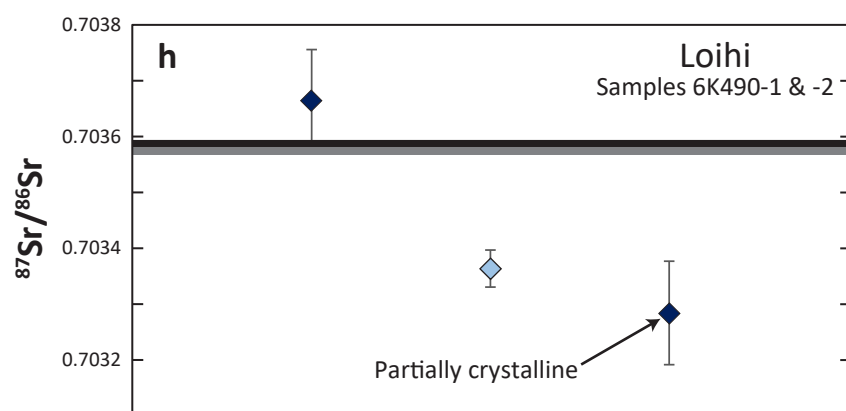
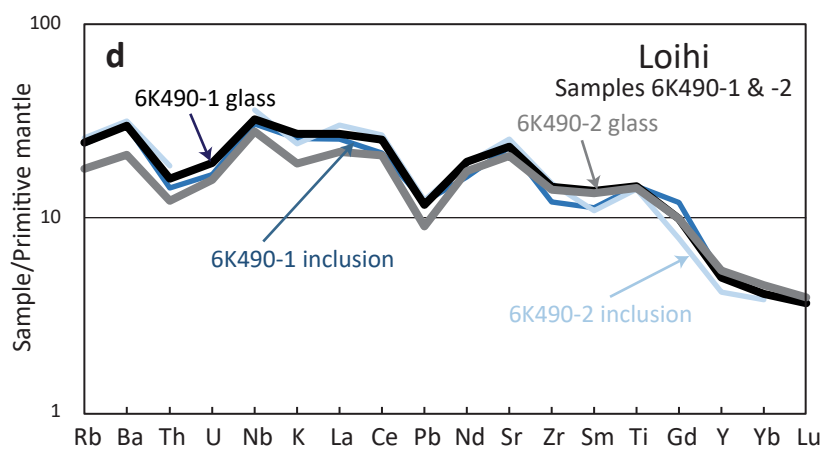
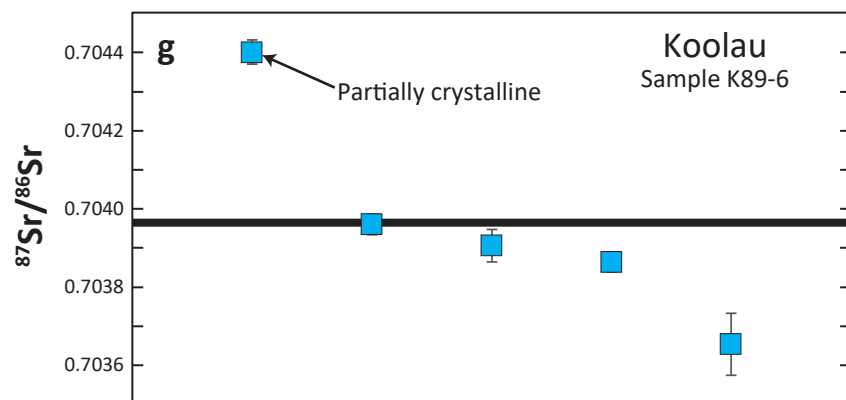
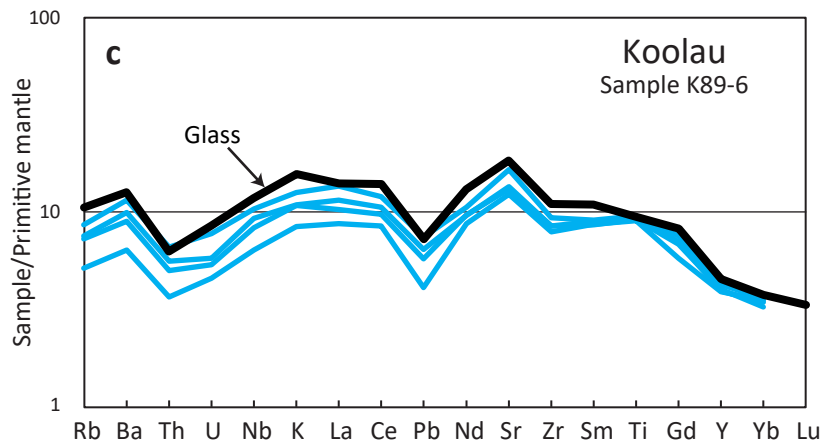
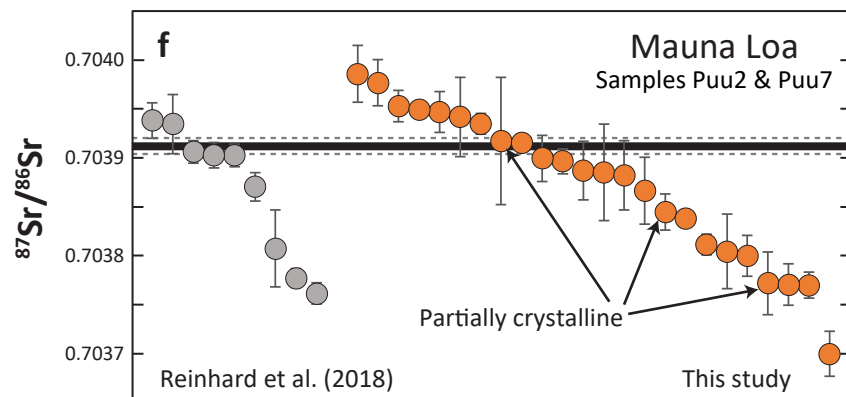
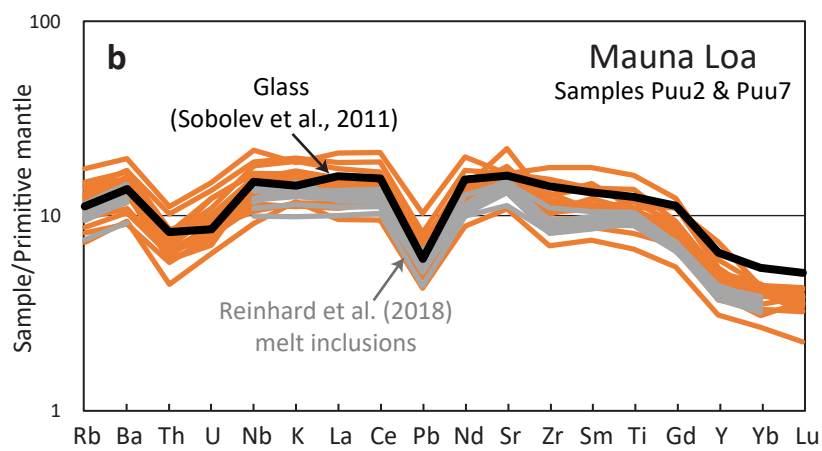
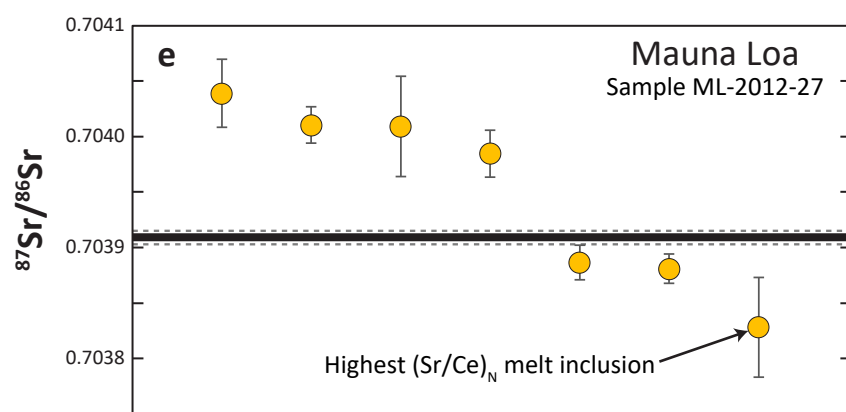
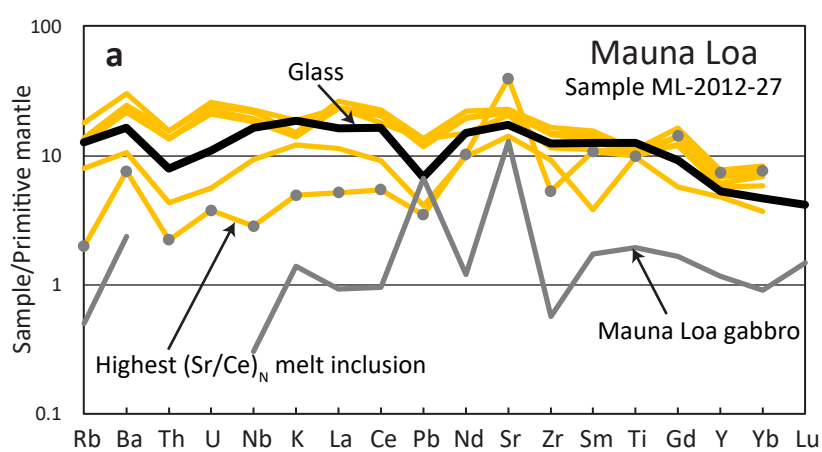
- High $(\text{Sr}/\text{Ce})_N$ melt inclusions (Sobolev et al., 2000, 2011)
- Ultra-depleted melt (UDM) inclusions (Sobolev et al., 2011)
- Low $(\text{Sr}/\text{Ce})_N$ Mauna Loa melt inclusions (Sobolev et al., 2000, 2011)
- Pu'u Wahi melt inclusions (Reinhard et al., 2018)
- Mauna Loa gabbros (Gaffney, 2002)
- Gabal Gerf gabbros (Zimmer et al., 1995)

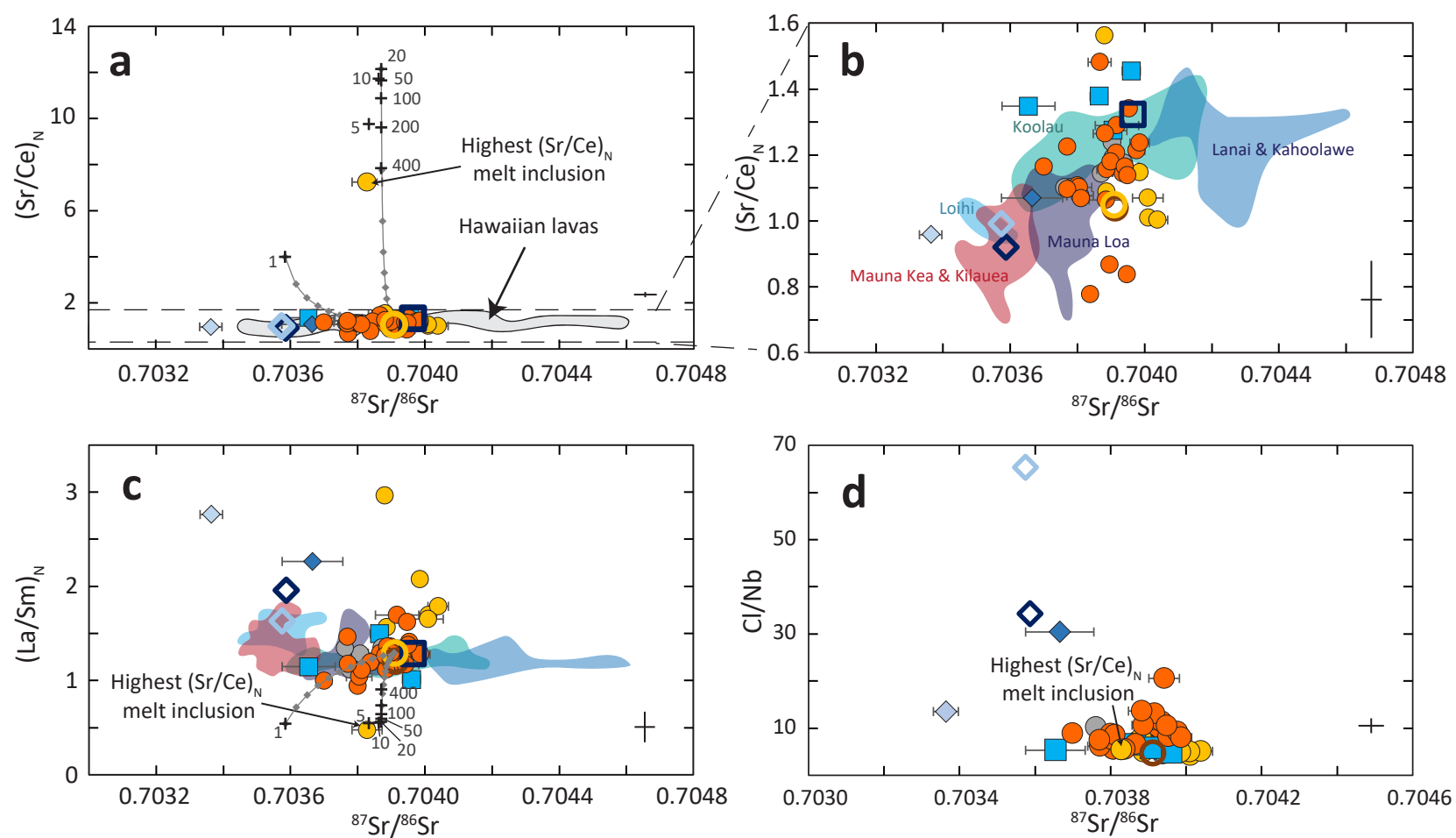


Sample	Melt inclusions	Glass	Volcano
ML-2012-27			Mauna Loa
Puu2 & Puu7			
6K490-1			Loihi
6K490-2			
K89-6			Koolau

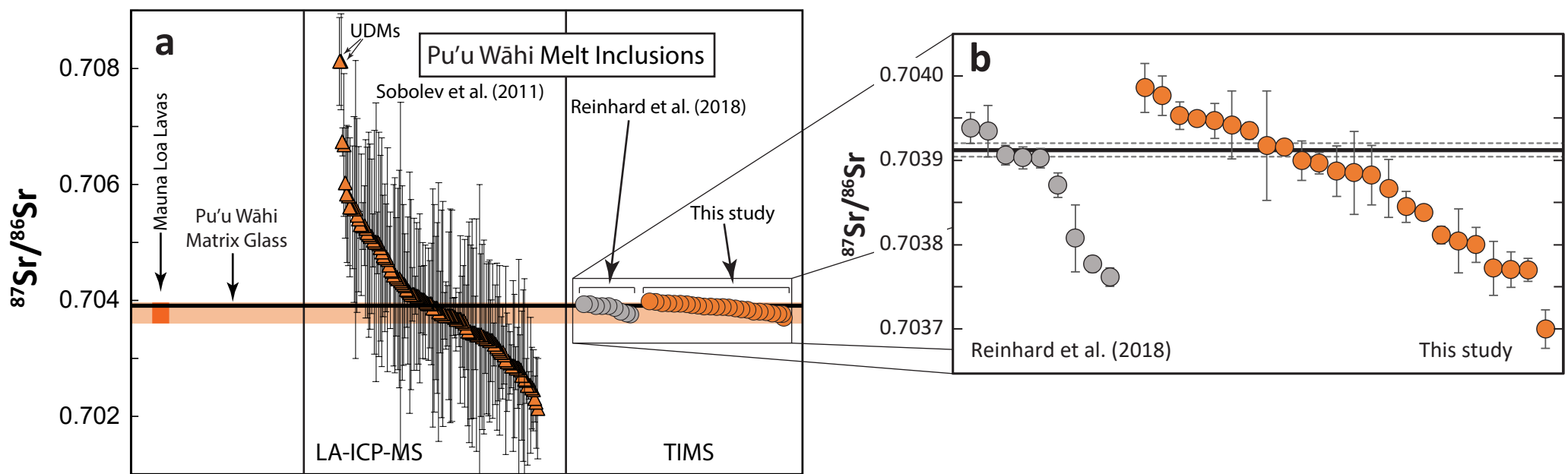
Previously published data

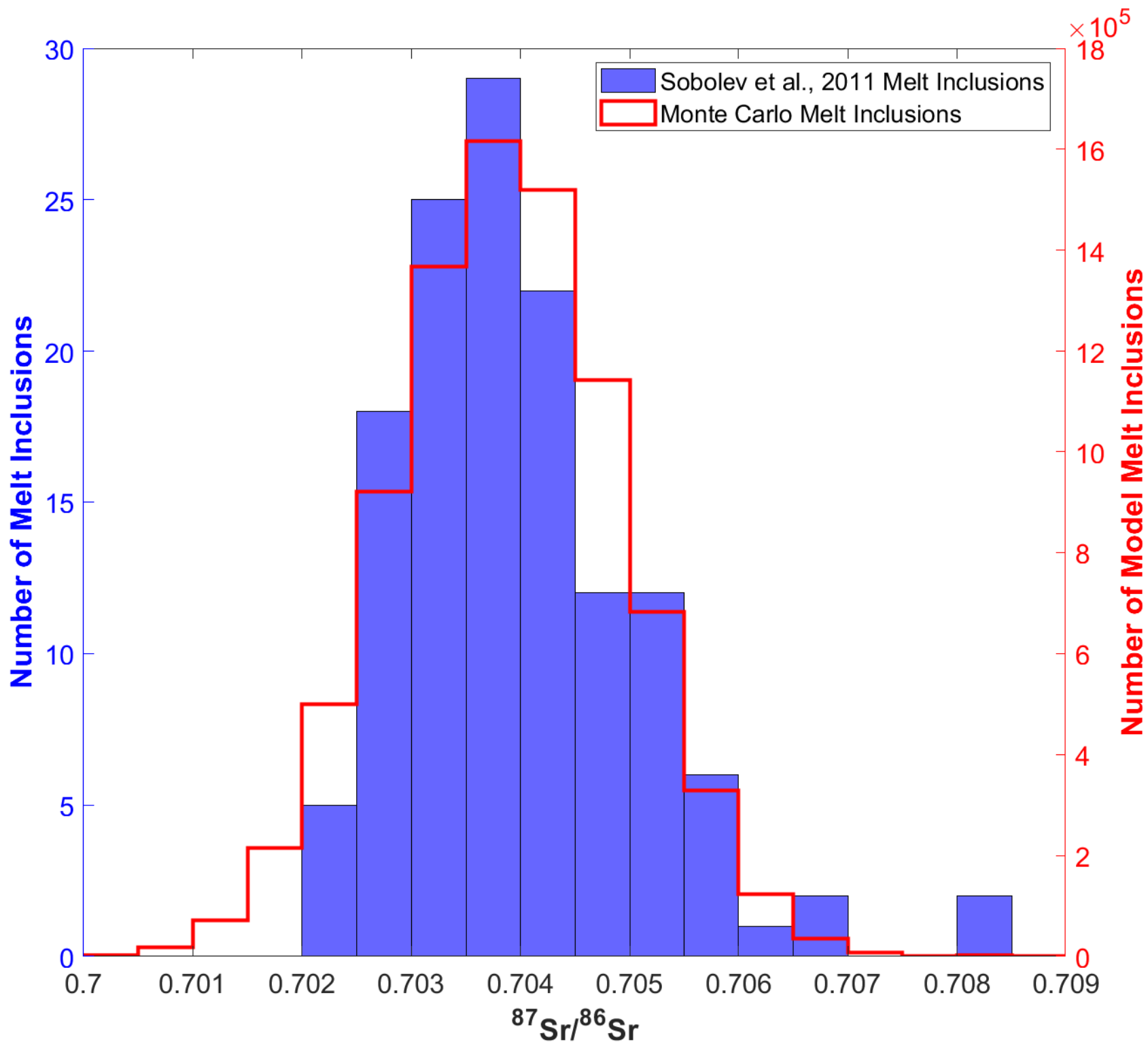
- High (Sr/Ce)_N melt inclusions (Sobolev et al., 2000, 2011)
- Ultra-depleted melt (UDM) inclusions (Sobolev et al., 2011)
- Low (Sr/Ce)_N Mauna Loa melt inclusions (Sobolev et al., 2000, 2011)
- Pu'u Wahi melt inclusions (Reinhard et al., 2018)
- Mauna Loa gabbros (Gaffney, 2002)
- Gabal Gerf gabbros (Zimmer et al., 1995)





Sample	Melt inclusions	Glass	Volcano
ML-2012-27	●	○	Mauna Loa
Puu2 & Puu7	●	○	Mauna Loa
6K490-1	◆	◇	Loihi
6K490-2	◆	◇	Loihi
K89-6	■	□	Koolau
Previously published data			
● Pu'u Wahi melt inclusions (Reinhard et al., 2018)			





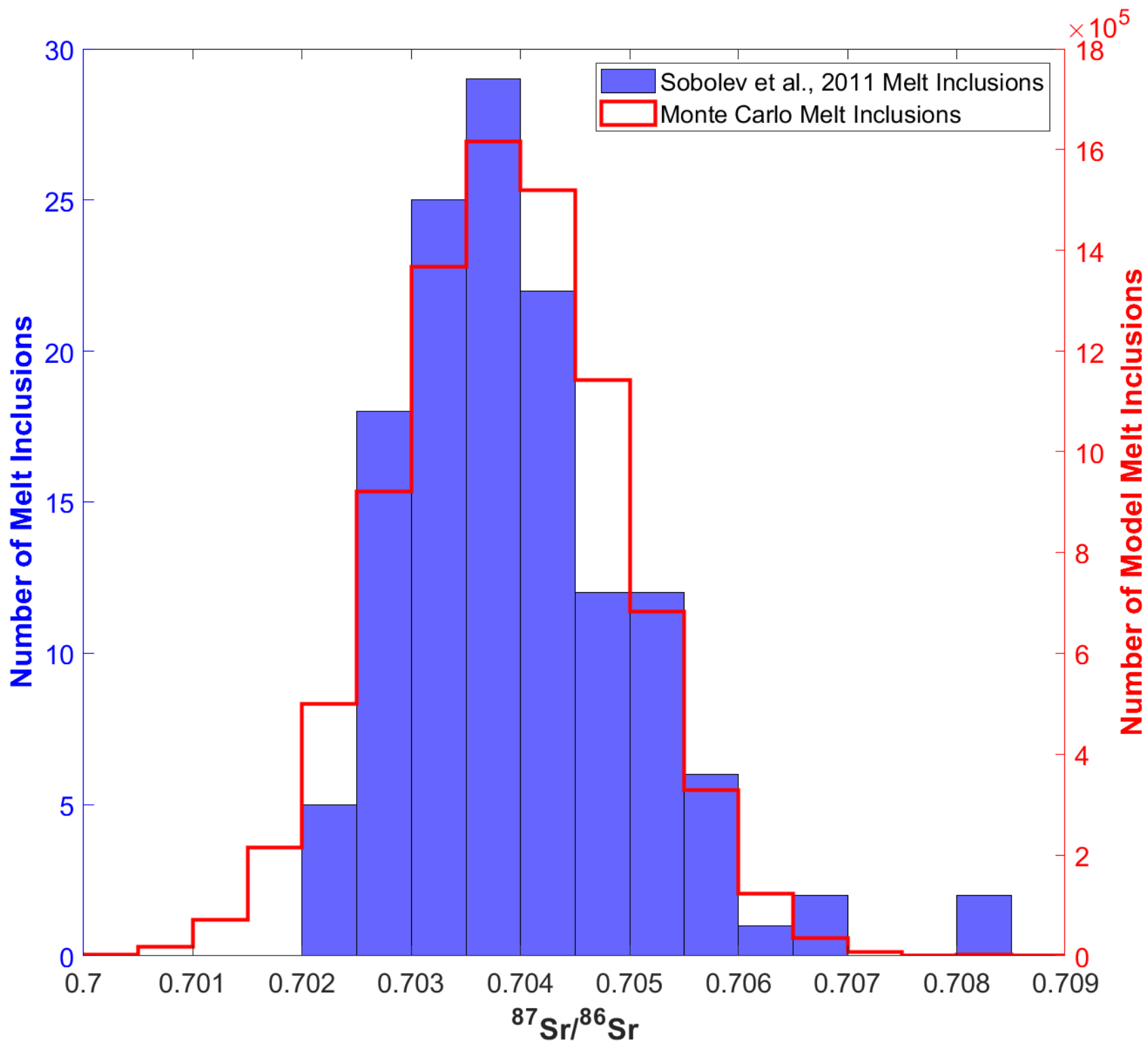


Table 1. $^{87}\text{Sr}/^{86}\text{Sr}$ measurements made on melt inclusions and the glass of the host lava in this study.

Sample	Sr (ppm)	Ce (ppm)	(Sr/Ce) _N	Total Sr (ng)	[Sr] _{sample} /[Sr] _{blank}	$^{87}\text{Sr}/^{86}\text{Sr}^a$	2σ (std. err.)	ppm change in $^{87}\text{Sr}/^{86}\text{Sr}$ ratio from blank correction ^b
Mauna Loa - Pu'u Wahi (Puu2 & Puu7)								
Puu2-1-2	-	-	-	2.5	222	0.703772	0.000032	46
Puu2-1-9	270	20.6	1.11	15.5	292	0.703800	0.000021	35
Puu2-1-18a	337	26.7	1.06	2.8	53	0.703885	0.000049	191
Puu2-1-19	338	24.1	1.18	1.1	97	0.703899	0.000024	104
Puu2-1-39	215	15.8	1.14	7.3	1038	0.703935	0.000010	10
Puu7-1-20	438	24.9	1.48	1.2	177	0.703867	0.000034	57
Puu7-2-15	-	-	-	3.7	527	0.703845	0.000018	19
Puu7-2-92b	-	-	-	0.9	78	0.703917	0.000065	129
Puu7-2-80	324	20.3	1.34	9.2	817	0.703953	0.000016	12
Puu7-2-19	325	35.2	0.78	18.9	2690	0.703838	0.000008	4
Puu7-1-29	330	25.2	1.10	1.2	168	0.703804	0.000038	61
Puu7-3-19a	314	21.9	1.21	17.5	329	0.703916	0.000009	31
Puu7-3-31	265	19.1	1.16	28.8	542	0.703700	0.000023	19
Puu7-1-14	279	28.0	0.84	3.6	67	0.703947	0.000021	149
Puu7-1-30	325	31.6	0.87	2.5	46	0.703896	0.000013	218
Puu7-1-36	338	25.9	1.10	23.5	441	0.703770	0.000014	23
Puu7-2-62	334	24.3	1.16	3.1	444	0.703887	0.000030	23
Puu7-1-41	330	22.8	1.21	7.7	682	0.703977	0.000023	15
Puu7-2-6	327	25.8	1.07	9.8	1400	0.703811	0.000010	7
Puu7-2-40a	280	19.2	1.22	9.6	855	0.703770	0.000021	12
Puu7-2-42	336	22.9	1.24	5.3	469	0.703986	0.000029	21
Puu7-2-7a	311	22.5	1.16	3.1	445	0.703942	0.000040	23
Puu7-1-10	355	26.3	1.14	13.5	1923	0.703949	0.000008	5
Puu7-2-52	345	23.0	1.26	5.0	447	0.703882	0.000035	23
host glass^c	319	25.9	1.04			0.703912	0.000008	
Mauna Loa ML-2012-27								
ML-2012-27_2	283	15.3	1.56	10.0	1027	0.703881	0.000013	10
ML-2012-27_5a	457	38.1	1.01	10.2	1042	0.704010	0.000016	10
ML-2012-27_7	441	34.1	1.09	2.9	300	0.703887	0.000016	34
ML-2012-27_18a	426	35.8	1.00	0.7	69	0.704039	0.000030	144
ML-2012-27_21a	437	34.4	1.07	1.8	181	0.704009	0.000045	55
ML-2012-27_25	411	30.2	1.15	2.1	215	0.703985	0.000021	46
ML-2012-27_19b	786	9.1	7.24	1.4	74	0.703828	0.000045	137
host glass	344	27.6	1.05			0.703909	0.000006	
Koolau - K89-6								
K89-6_52	-	-	-	3.5	363	0.704401	0.000031	26
K89-6_53	260	16.2	1.35	0.5	25	0.703654	0.000079	416
K89-6_55	244	14.1	1.45	10.5	1495	0.703960	0.000027	7
K89-6_65	327	20.0	1.38	1.4	86	0.703864	0.000026	118
K89-6_76a	267	17.6	1.27	0.6	65	0.703906	0.000041	155
host glass	366	23.3	1.32			0.703965	0.000006	
Loihi - 6K490-1								
6K490-1_51	-	-	-	0.9	52	0.703284	0.000093	211
6K490-1_78	459	36.1	1.07	0.3	31	0.703665	0.000090	339
host glass	460	42.1	0.92			0.703586	0.000006	
Loihi - 6K490-2								
6K490-2_79a	507	44.5	0.96	1.1	63	0.703363	0.000033	173
host glass	412	35.0	0.99			0.703574	0.000006	

Note: The Sr and Ce fractionation-corrected concentrations are reported here, but not for partially crystalline inclusions.

^a $^{87}\text{Sr}/^{86}\text{Sr}$ values have been blank corrected and corrected for the offset between the preferred (0.710240) and the measured $^{87}\text{Sr}/^{86}\text{Sr}$ of NBS987.

^b The change in $^{87}\text{Sr}/^{86}\text{Sr}$ ratio due to the blank correction (ppm) is calculated as $(^{87}\text{Sr}/^{86}\text{Sr}_{\text{meas-norm987}} - ^{87}\text{Sr}/^{86}\text{Sr}_{\text{blank-corrected}}) / ^{87}\text{Sr}/^{86}\text{Sr}_{\text{meas-norm987}} * 10^6$.

^c Sr concentration and $^{87}\text{Sr}/^{86}\text{Sr}$ of Pu'u Wahi glass is from Reinhard et al. (2018).

Table 2. Model parameters and output data for the diffusive interaction model based on the model of Peterson et al. (2014).

	$K_d(\text{plag-melt})^a$	$D_{\text{plag}} (1200^\circ\text{C}, \text{m}^2 \text{s}^{-1})^b$	Plagioclase melt ^c (ppm)	Initial melt ^d (ppm)	Output data (concentrations in ppm)							
					1 year	5 years	10 years	20 years	50 years	100 years	200 years	400 years
Ba	0.230	8.09E -19	198	4.69	4.86	5.52	6.35	7.99	12.82	20.57	35.03	60.18
Th	0.050	3.10E -21	1.37	0.07	0.07	0.07	0.07	0.07	0.07	0.07	0.07	0.07
U	0.024	3.10E -21	0.47	0.03	0.03	0.03	0.03	0.03	0.03	0.03	0.03	0.03
Nb	0.030	3.10E -21	20.4	1.24	1.24	1.24	1.24	1.24	1.24	1.24	1.24	1.24
K	0.171	4.38E -16	7222	408	2364	5618	6368	6491	6494	6494	6494	6494
La	0.106	3.87E -19	21	1.60	1.60	1.62	1.64	1.67	1.78	1.96	2.32	3.01
Ce	0.081	3.87E -19	53.5	4.57	4.58	4.61	4.64	4.71	4.92	5.28	5.97	7.32
Pb	0.511	1.41E -17	1.69	0.15	0.23	0.52	0.80	1.17	1.55	1.63	1.63	1.63
Nd	0.084	2.92E -19	36	4.76	4.77	4.78	4.80	4.83	4.94	5.11	5.46	6.14
Sr	1.813	3.37E -17	689	63.5	217	534	647	680	682	682	682	682
Zr	0.004	3.10E -21	264	41.5	41.5	41.5	41.5	41.5	41.5	41.5	41.5	41.5
Hf	0.015	3.10E -21	6.33	1.27	1.27	1.27	1.27	1.27	1.27	1.27	1.27	1.27
Sm	0.056	2.92E -19	9.3	1.88	1.88	1.88	1.88	1.89	1.90	1.93	1.99	2.10
Eu	0.534	2.92E -19	3.06	0.74	0.83	1.13	1.39	1.67	1.88	1.94	2.01	2.15
Ti	0.076	3.10E -21	21049	5310	5310	5311	5311	5311	5311	5312	5314	5317
Dy	0.019	3.24E -19	6.77	3.37	3.58	3.58	3.58	3.58	3.58	3.58	3.58	3.58
Yb	0.015	5.06E -19	2.09	2.04	2.04	2.04	2.04	2.04	2.04	2.04	2.04	2.04
⁸⁷ Sr/ ⁸⁶ Sr			0.703872	0.702569	0.703585	0.703833	0.703863	0.703870	0.703871	0.703871	0.703871	0.703871

For the diffusion model we assume that the plagioclase grain size is 0.001 m, there is 1% melt, and 50% of the solid is plagioclase.

^aBédard (2006) for plagioclase of An₈₀ at 1200°C

^bDiffusion coefficients for plagioclase at 1200°C from Cherniak and Watson (1994), Giletti and Casserly (1994), Cherniak (1995, 2002, 2003) and Giletti and Shanahan (1997). However, some trace elements do not have experimentally determined diffusion coefficients. For trace elements without this data, Peterson et al. (2014) estimated based on cation size and charge (Behrens et al., 1990; Saal and Van Orman, 2004). Peterson et al. (2014) assumed that the diffusion coefficients for Nb, Zr, and Ti are similar to those of Th and U. Like Peterson et al. (2014), we assumed that Eu is 50% Eu²⁺, and that the diffusion coefficient for Eu²⁺ is similar to that of Sr.

^c While Peterson et al. (2014) used a Galapagos lava to calculate an equilibrium plagioclase composition, we use a Mauna Loa lava (Mauna Loa sample J2-15-13; Wanless et al., 2006). The plagioclase composition in equilibrium with this melt is calculated using the partition coefficients in the table.

^d Like Peterson et al. (2014), the initial melt is a 12% aggregated fractional melt of DMM composition from Workman and Hart (2005), and the isotopic value is the average of the East Pacific Rise Ridge segment averages from Gale et al. (2013).